Quaternary International 384 (2015) 52–81

Contents lists available at ScienceDirect

Quaternary International

journal homepage: www.elsevier.com/locate/quaint

Last Glacial Maximum climate over Korean Peninsula in PMIP3 simulations

Seong-Joong Kim*, Ji-Won Kim, Baek-Min Kim

Korea Polar Research Institute, KORDI, PO Box 32, Incheon 406-840, South Korea

ARTICLE INFO

Article history:
Available online 26 March 2015

Keywords:
Climate change
Last Glacial Maximum
Korea
PMIP3

ABSTRACT

The Last Glacial Maximum (LGM) at 21,000 years before present is a marked climate event with thick ice sheets over North America and Europe and associated sea level drop of about 120 m. We used the most updated coupled climate model results to analyze the climate change over Korea for the LGM. Eight coupled models (CCSM, CNRM, COSMOS, FGOALS, IPSL, MIROC, MPI, and MRI) were used to analyze the LGM climate. With LGM boundary conditions, surface air temperature decreases almost everywhere in all seasons with the largest cooling in winter and least cooling in summer. Overall, in the LGM, the multi-model annual-mean cooling over Korea is 5.85 C°, which is consistent with proxy evidence using pollen reconstructions. Associated with the surface cooling, precipitation decreases in general, with the largest reduction in winter by 56%, but in summer precipitation increases by 12% in the LGM over Korea. Overall, precipitation decreases by about 14% in the LGM over Korea. The surface cooling tends to increase surface pressure almost everywhere over Asia. The sea level pressure increase is especially larger in high latitudes and this leads to the easterly wind anomaly in northern part of Korea. On the other hand, in South Korea, the increase in surface pressure leads to the westerly wind anomaly. The increase in surface pressure associated with surface cooling leads to the anticlockwise wind anomalies in the LGM over Korea.

1. Introduction

The Last Glacial Maximum (LGM) at 21,000 BP is one of the largest climate events in earth's climate history. Initiated by the seasonal energy deficit in the Northern Hemisphere by orbital parameters at about 115 ka, the ice sheet had continuously grown to 4 km thickness until 21,000 BP, and sea level had been lowered by about 120 m on average (IPCC, 2013). There have been numerous efforts in reconstructing the LGM temperature using proxy data over the ocean (MARGO Project Members, 2009) and over land (Bartlein et al., 2011). In the LGM, the largest ocean surface cooling occurred in the North Atlantic, where sea surface temperature (SST) dropped by 10 C°. The large surface ocean cooling over the North Atlantic is associated with the southward expansion of sea ice in the LGM. In the Mediterranean and the Southern Ocean, SST decreased by 6 C° and 2–6 C°, respectively (MARGO Project Members, 2009). The degree of SST change over the tropics has been controversial and tends to depend on the proxy data (Kim et al., 2003). The IPCC AR5 report (2013) suggested that one group shows relatively less cooling in the tropics by 0.3–2.7 C° (MARGO Project Members, 2009), whereas another group suggests moderate cooling by 2.2–3.2 C° in the LGM (Ballantyne et al., 2005).

In the LGM, surface air temperature (SAT) reduction compared to modern conditions is larger than SST decrease. For example, in the LGM, the largest surface cooling occurred over Greenland, 21–25 C° based on borehole paleothermometry (Cuffey et al., 1995) and the second largest cooling in east Antarctica, 7–10 C° (Stenni et al., 2010; Uemura et al., 2012). The surface cooling in the LGM elsewhere ranges from 3.9 to 4.6 C° (Shakun et al., 2012).

Although there have been many efforts in reconstructing surface climate over high latitudes, North America and Europe using various proxies, the degree of climate change over Korea for the LGM has not been studied comprehensively and thoroughly. The Korean Peninsula is surrounded by ocean, but the West Sea is generally shallower than the sea level drop in the LGM (about 120 m), and thus the West Sea was exposed to land in the LGM. This exposure might result in substantial cooling due to much lower heat capacity. In the southern part, the Korea Strait is approximately 130 m deep, and this sill depth might have allowed partial

* Corresponding author.
E-mail address: seongjkim@kopri.re.kr (S.-J. Kim).

http://dx.doi.org/10.1016/j.quaint.2015.02.062
1040-6182/

entry of water to the East Sea in the LGM. As the East Sea surface temperature is largely influenced by the warm water influx from the Kuroshio Current, the partial limitation of the warm water influx due to sea level drop might result in substantially different climate over Korea in the LGM.

Climate reconstruction of the LGM using proxy data is ideal, but often proxy data are limited in reconstructing quantitative change of climate, and most proxy data provide qualitative assessments over Korea in the LGM. Alternatively, numerical simulation of the LGM can help quantify climate change, and numerical models could be tested against known past climate fluctuations to have confidence in their predicting skill for future climate change. The LGM climate events provide the optimal opportunity to examine the Earth's climate change mechanisms, because paleoclimate proxy data are relatively abundant.

Using age-controlled pollen record from wetland Hannam, western central Korea, Yi and Kim (2010) found that during last glacial time cold and dry conditions prevailed with the expansion of subalpine coniferous forest and high aridity. These proxy re-constructions provide useful information for the climate and environment conditions for the two periods. A comparison with numerically reproduced results with these proxy re-constructions will be useful for understanding climate change mechanism in quantitative sense. In this study, we use the most updated numerical model results to investigate the change in temperature and hydrological budget for the LGM. We compare the reproduced results with proxy reconstructions.

2. Model description and experiments

In this study, we used the model results from the third phase of the Paleoclimate Modelling Intercomparison Project (PMIP3), which was performed to understand climate change mechanisms (Braconnot et al., 2012), identify the different climatic factors, and evaluate past and present climate for the IPCC AR5 (2013). In order to analyze climate change over Korea in the LGM, we used eight numerical models of CCSM4, CNRM-CM5, IPSL-CM5A-LR, COSMOS-ASO, FGOALS-g2, MIROC-ESM, MPI-ESM-P, and MRI-CGCM3. A more detailed explanation on the PMIP3 is found at https://pmip3.lsce.ipsl.fr.

The modern climate simulation, called PI (pre-industrial), is forced by contemporary trace gases, vegetation, ice sheets, and solar constant (see Table 1). The PI run is the same as the one used for the fifth phase of Coupled Model Intercomparison Project (CMIP5). Vegetation is computed interactively using different vegetation models. In CCSM4, biophysical processes are computed in the community land model version 4 (CLM4) where solar long wave radiation interacts with vegetation, which is dynamic. In CNRM CM5, the natural land surface scheme based on “Interaction between soil and biosphere and atmosphere model” is included. In IPSL, the land surface model includes energy and water cycle of soil and vegetation, terrestrial carbon cycle, vegetation composition and distribution with 12 plant functional types and bare soil. In COSMOS-ASO and MPI-ESM-P, biogeochemical and biogeophysical process from terrestrial processes are included in the dynamics vegetation module including fire and land use change. The FGIALS-2 model uses a dynamics vegetation module, called VEGAS 2.0, with soil and temporal evolution of terrestrial vegetation, 5 plant functional types, and land use and fire. In the MIROC-ESM model, a process-based terrestrial ecosystem model of global dynamic vegetation dynamics and terrestrial carbon cycling with 13 plant functional types and 2 organic carbon pools is used. In the MRI-CGCM3, a model of surface vegetation process with 2 vegetation layers, evapotranspiration processes is included.

Table 1
PMIP3 forcing and boundary conditions for the preindustrial and LGM simulations.

	Preindustrial	LGM
CO_2 (ppm)	280	185
CH_4 (ppb)	760	350
N_2O (ppb)	270	200
Eccentricity	0.16724	0.018994
Obliquity	23.446	22.949
Precession	102.04	114.42
Ice sheet	Present	Blended ice sheet
Land Mask	Present	Prescribed from blended ice sheet
Salinity	Calculated	+1 PSU everywhere
Vegetation	Computed or prescribed to present	Computed or prescribed to present

To simulate LGM climate, all numerical models used orbital parameters for 21 ka (0.018994 for eccentricity, 22.949 for obliquity, and 114.42 for precession), atmosphere CO_2 concentration of 185 ppm, methane concentration of 350 ppb, nitrous oxide of 200 ppb. The same conditions as the PI are used for the ozone concentration, aerosols, solar constant. LGM vegetation conditions are the same as PI. Ice sheets were prescribed as the LGM ice sheet extent and related changes in topography with blended ice sheet models. A more detailed description of the LGM boundary conditions is found at the PMIP3 website. This experiment is referred to as LGM.

3. Simulated climate

3.1. Surface air temperature

During the LGM, atmosphere CO_2 concentration was lowered by about 80 ppm, a thick ice sheet, more than 3 km in some places, was present over North America and Europe, and the Antarctic ice sheet was thicker than present. Because of these factors, the climate is expected to be overall colder than pre-industrial. Fig. 1 presents the geographic distribution of the change in seasonal-mean and annual-mean surface air temperature (SAT) between LGM and PI reproduced from the PMIP3 models over Korea.

We examined seasonal variation of SAT changes to better understand which season contributes most to the annual-mean surface cooling. The largest surface cooling over Korea is reproduced in boreal winter (December–January–February) and the winter surface cooling is larger towards the south and west. The largest surface cooling is reproduced in the COSMOS-ASO model in the western part of South Korea, by more than 16 C° and the MIROC and CCSM models show relatively large cooling by more than 8 C° over almost the entire Korean Peninsula. The CNRM, FGOALS, IPSL, and MRI models tend to reproduce larger cooling over south and western South Korea. Overall, multi-model mean SAT reduction over Korea in the LGM winter is more than 8 C° in the southern part of Korea. In the northern part of North Korea, surface cooling is slightly smaller than the south.

In spring (March–April–May), surface cooling is slightly smaller than in winter. The largest spring surface cooling is reproduced in the MIROC model, especially in the northern part of Korea by more than 8 °C. All models show smaller surface cooling in the western part in spring. In CNRM and MRI general circulation models (GCMs), the least surface cooling occurs in the western part of the Korean Peninsula. Multi-model averaged surface cooling in spring is less than 4 C° in the western half of Korea, while surface cooling is more than 4 C° in the eastern half.

In summer (June–July–August), inter-model variations in surface temperature changes are larger than other seasons. The least

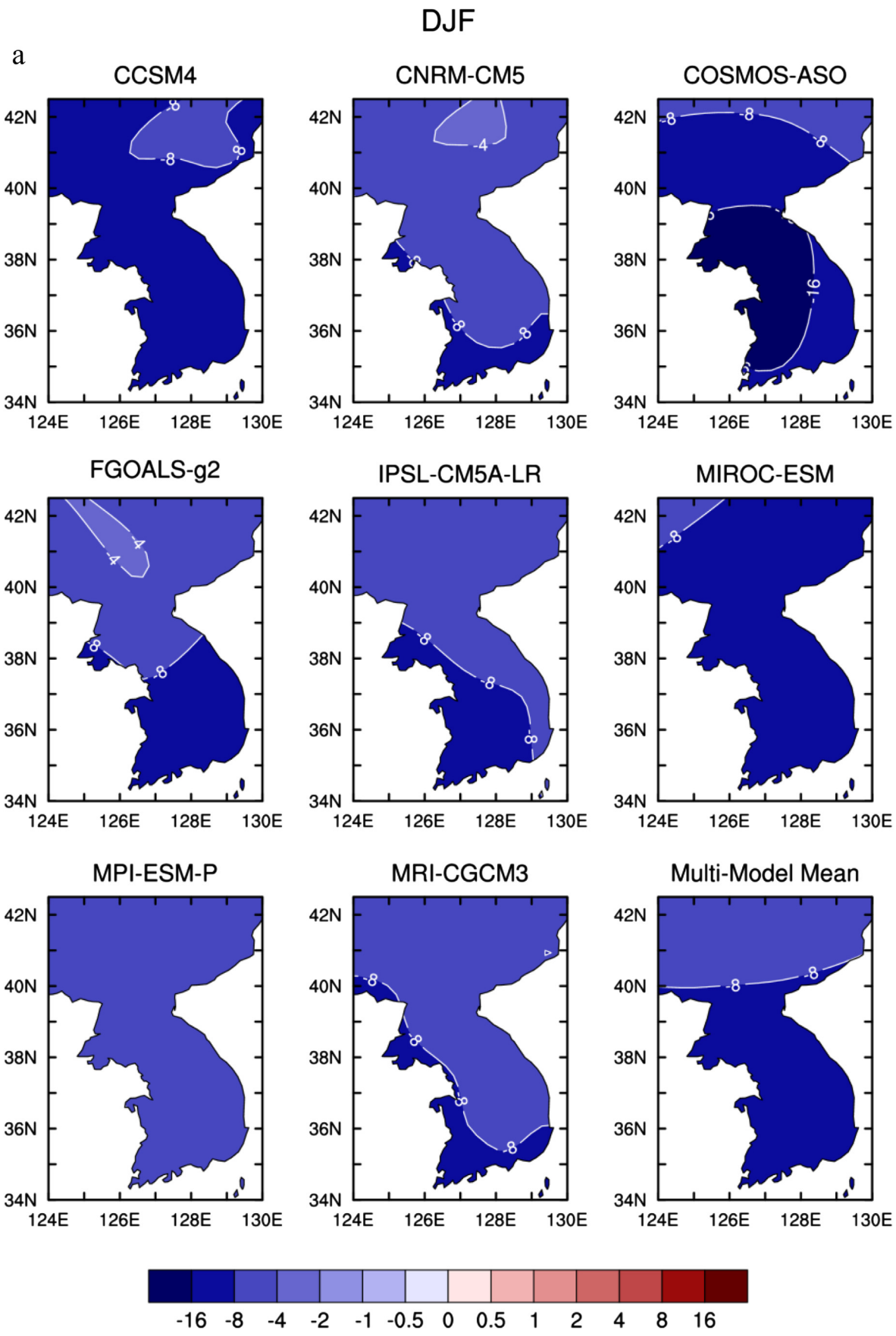

Fig. 1. Geographic distribution of the change in surface air temperature between the LGM and pre-industrial simulations for a) DJF, b) MAM, c) JJA, d) SON, e) annual-mean.

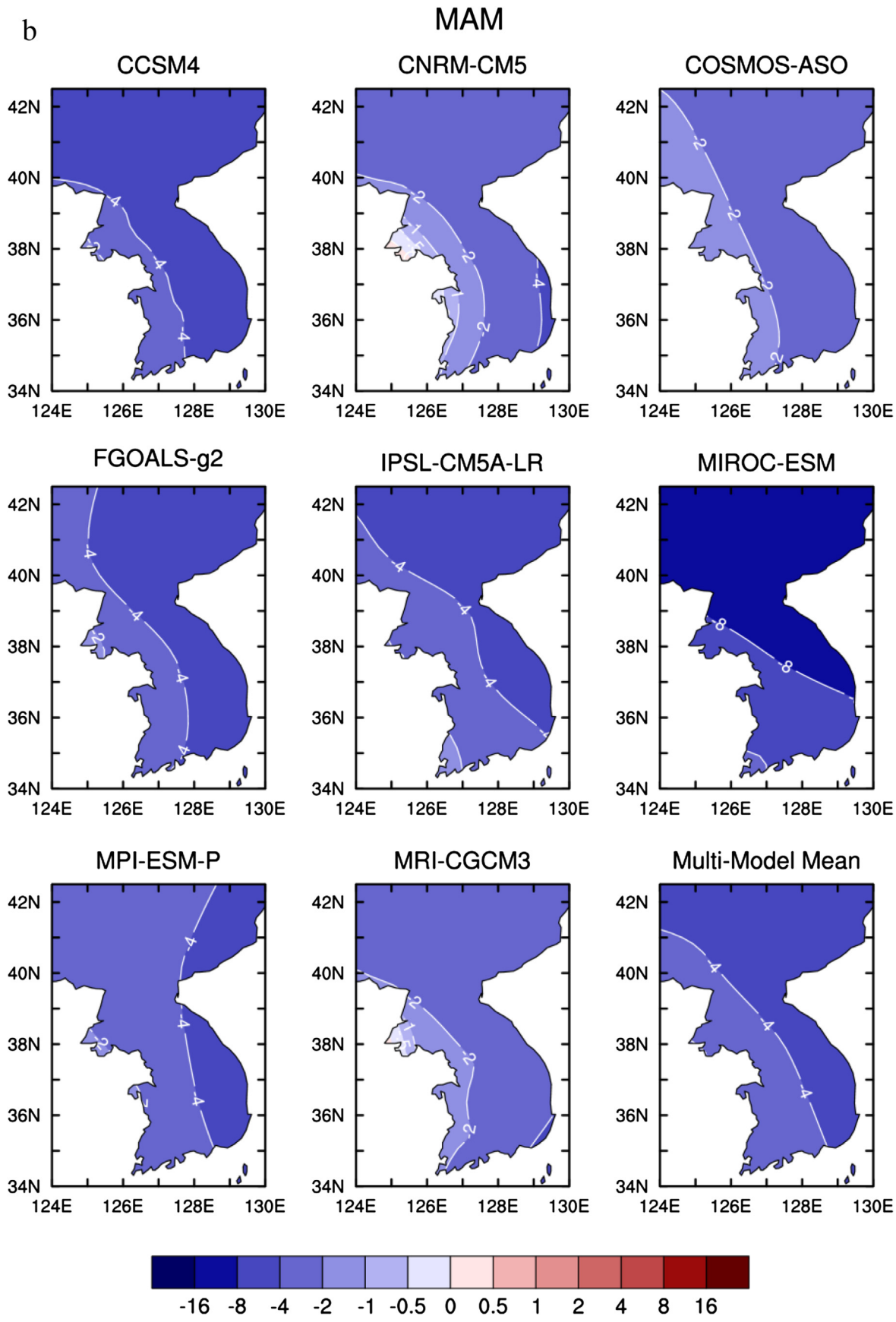

Fig. 1. (*continued*).

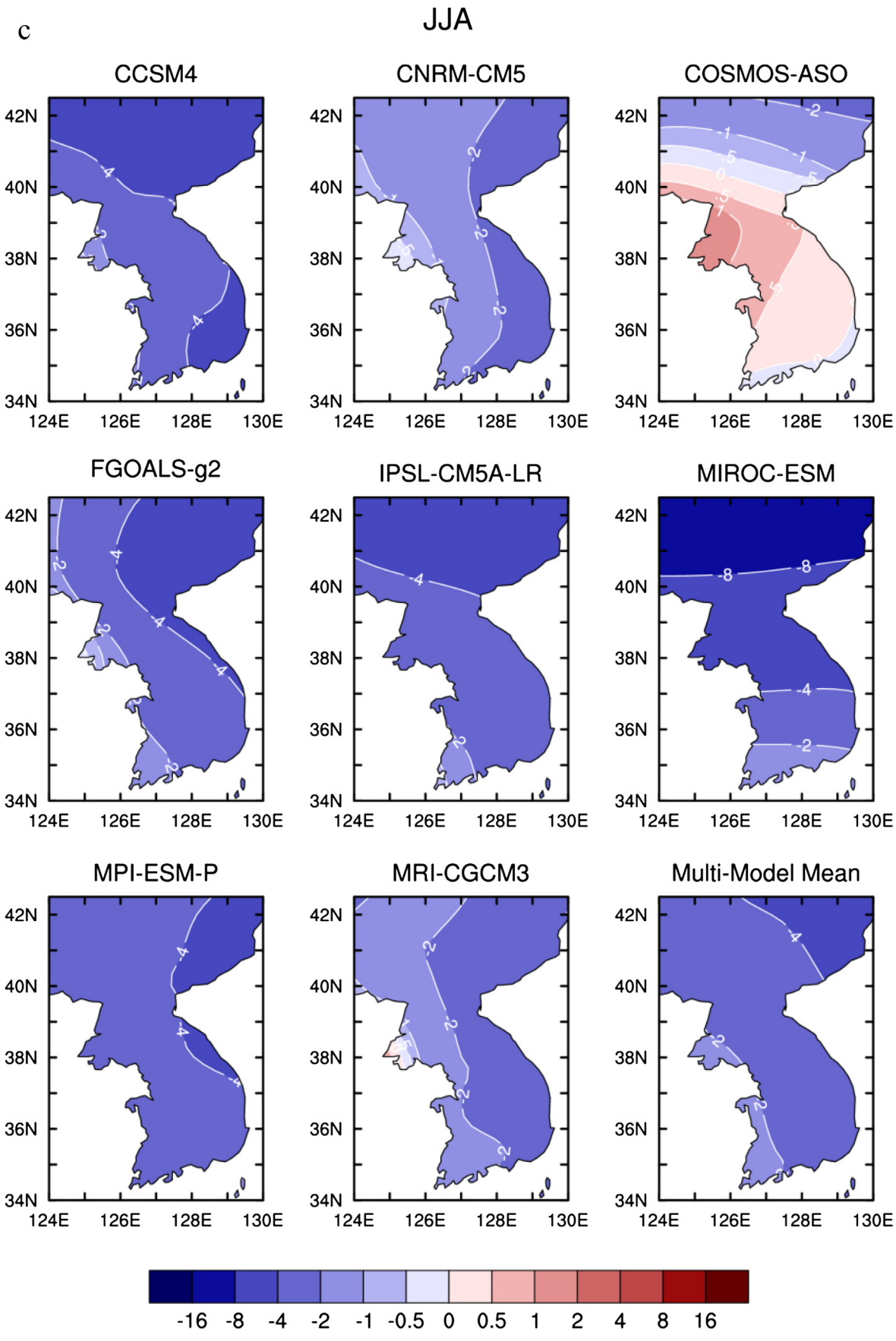

Fig. 1. (*continued*).

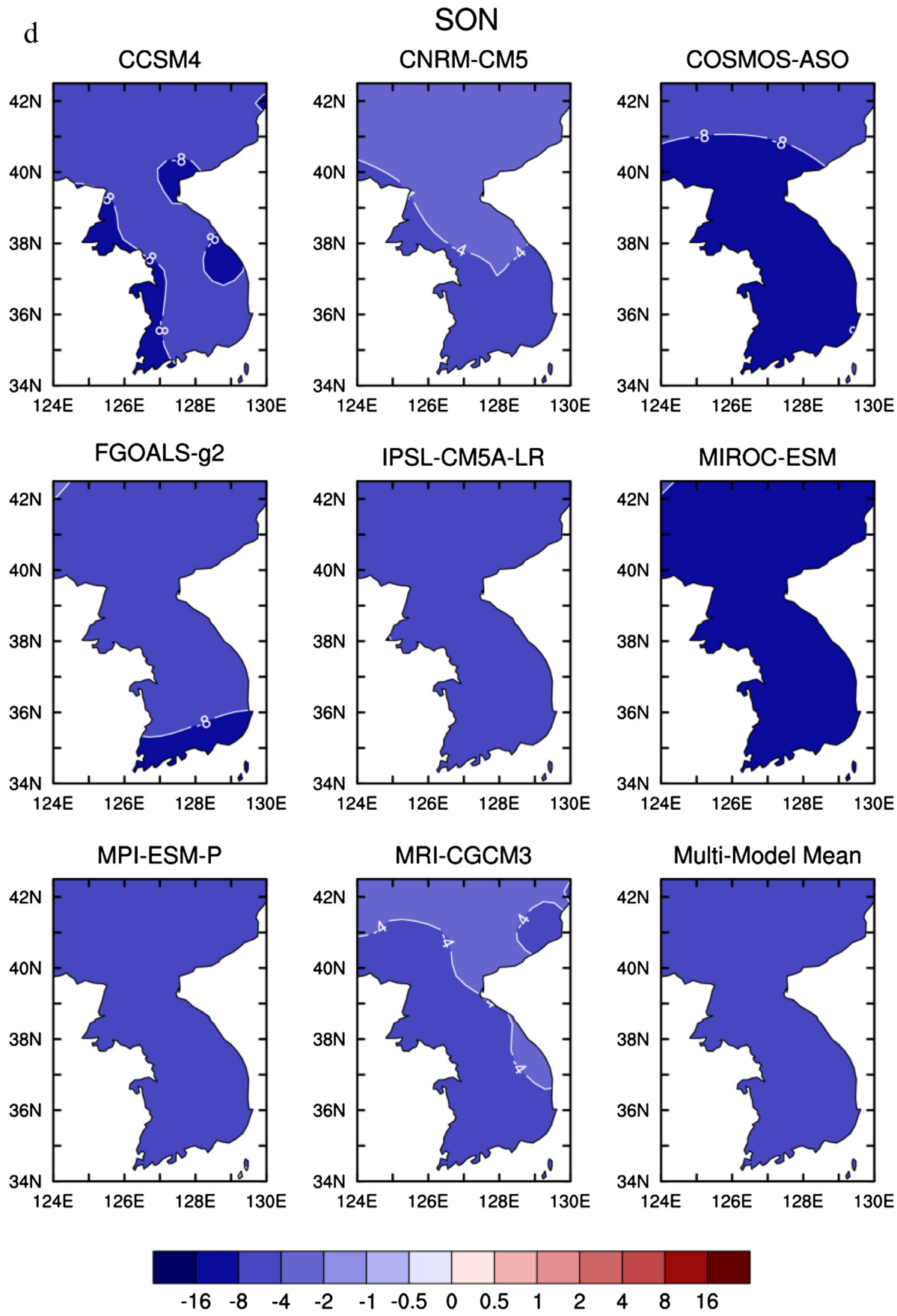

Fig. 1. (*continued*).

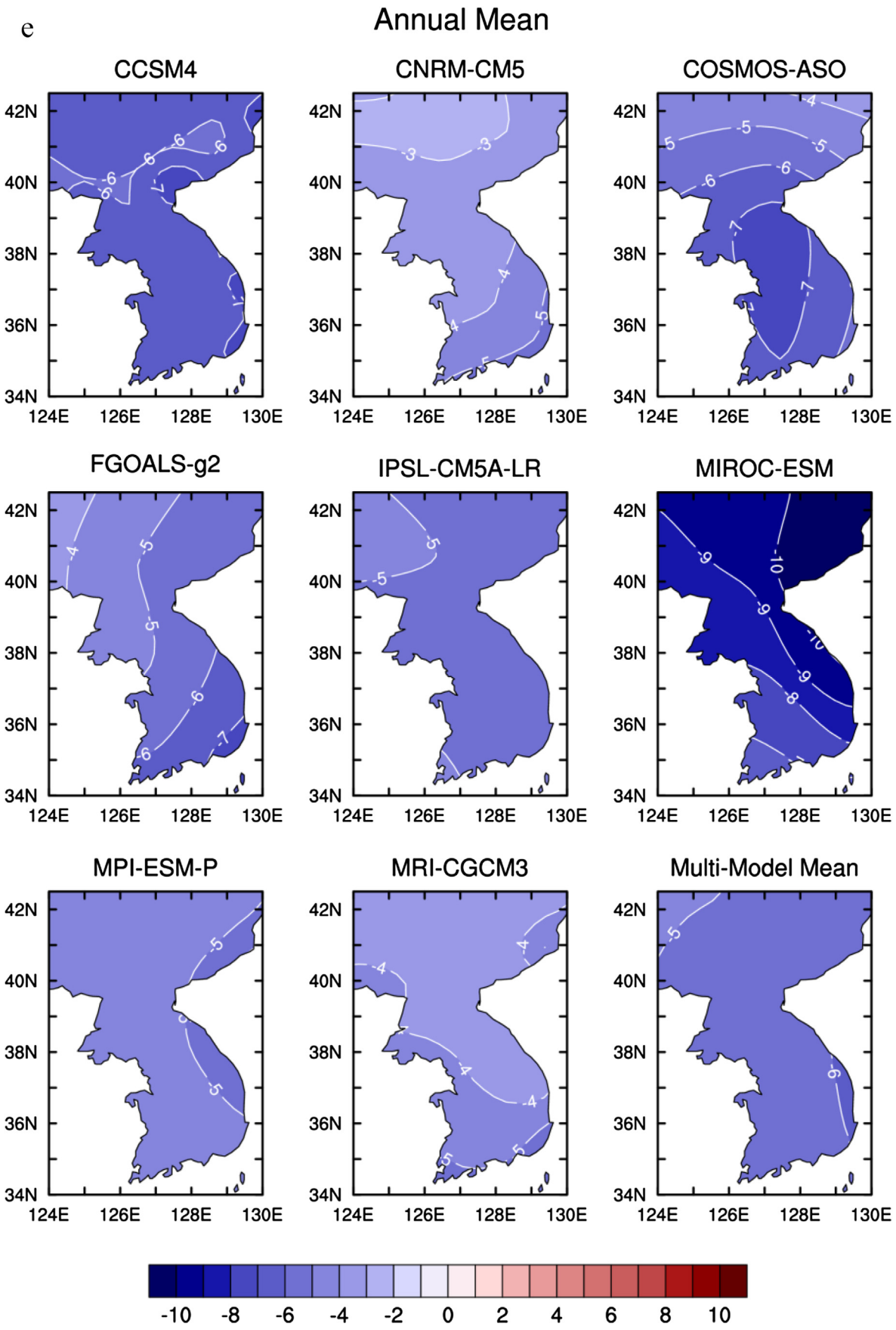

Fig. 1. (*continued*).

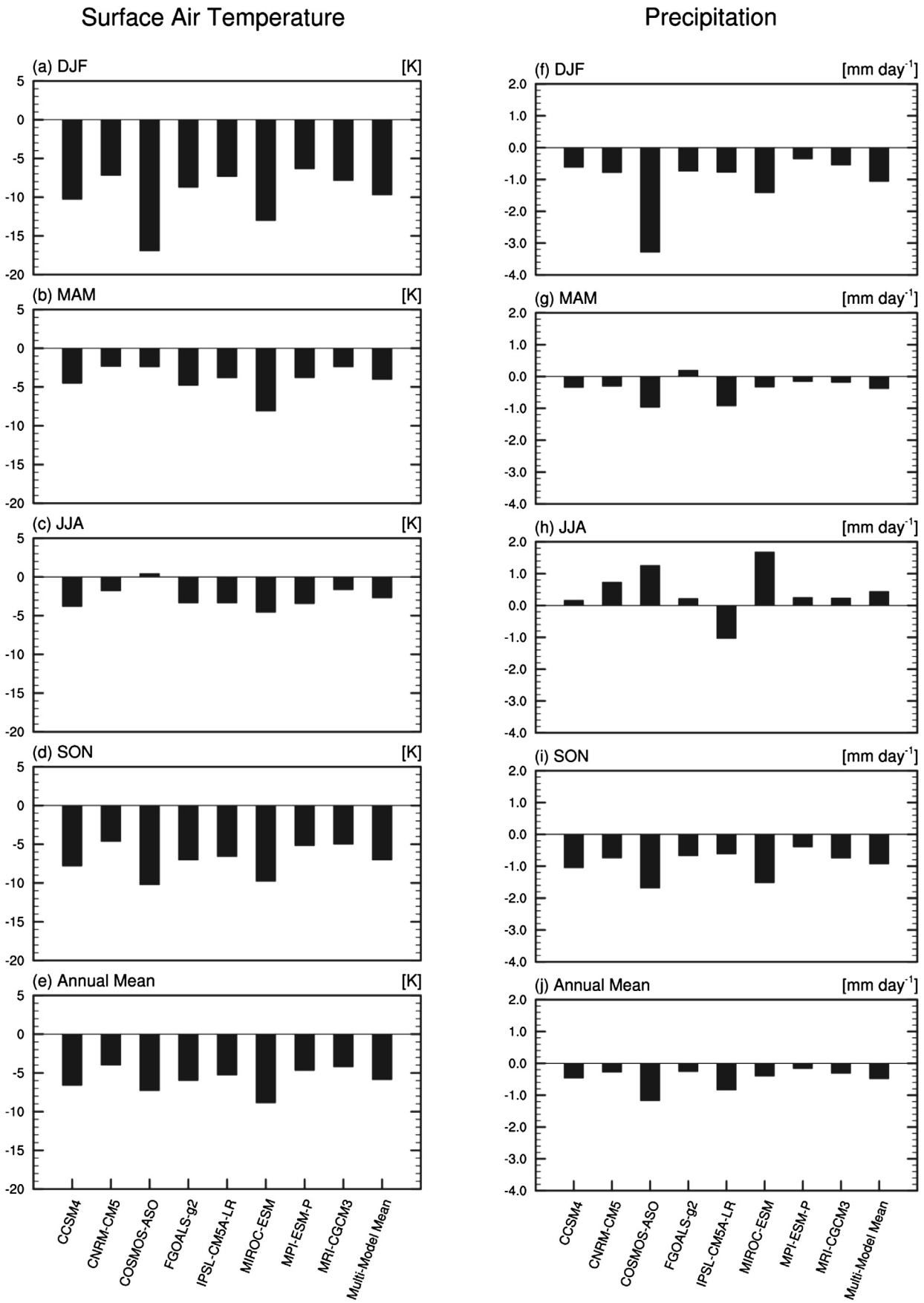

Fig. 2. Differences in surface air temperature averaged over Korea for a) DJF, b) MAM, c) JJA, d) SON, e) annual-mean and in precipitation for f) DJF, g) MAM, h) JJA, i) SON, j) annual-mean.

cooling occurs in the western part in most models. The COSMOS-ASO model shows a warming by more than 1 C° in the western part of 38°N. The MRI GCM also shows a slight warming in the same region. The surface cooling tends to be larger in the north of North Korea. The largest summer surface cooling, by more than 8 C°, is found in the MIROC GCM in the north of North Korea. Overall, multi-model mean summer surface cooling is less than 2 C° in the southwestern part of the Korean Peninsula, while medium range cooling by 2–4 C° occurs in the middle part. The largest cooling is found in the northeastern part of North Korea, by more than 4 C°.

In autumn (September–October–November), the surface cooling is slightly larger than in summer. In the southern part of peninsula, surface cooling is generally larger than in the north. Greater cooling is found in the MIROC and COSMOS models by more than 8 C°, while less surface cooling occurs in the CNRM and MRI GCMs, less than 4 C° in the northern part of Korea. Overall, in autumn, surface cooling is more than 4 C° for the entire peninsula.

Annual-mean temperature differences between the LGM and PI shows cooling over all of Korea, from less than 3 C° to more than 8 °C. The least annual-mean surface cooling is reproduced in northern Korea, by less than 3 C°in the CNRM-CM5, while the largest cooling of more than 10 C° is found in MIROC in northeastern Korea. Overall, multi-model annual-mean surface cooling over Korea ranges from 5 to 6 C° in the LGM.

Fig. 2 shows the regional mean difference in SAT over Korea between the two periods in different models. In winter, the largest surface cooling occurs in the COSMOS model by more than 15 C°, while the smallest winter cooling occurs in the MPI model, about 5 C°. Multi-model mean winter cooling is 9.7 C° in the LGM (Table 2). In spring, the surface cooling is much less than in winter. The largest cooling is reproduced in the MIROC model, more than 7 C°. The multi-model mean surface temperature reduction is 4 C° in spring. In summer, the surface cooling is even smaller than in spring time, with multi-model mean change of −2.7 C°. In autumn, the surface cooling over Korea is larger, with multi-model mean change of −7 C°. Overall, the annual-mean surface air temperature reduction over Korea in the LGM is 5.8 C°.

The range of surface temperature change over Korea is consistent overall with other previous PMIP model studies. Jiang et al. (2011) analyzed PMIP1 and PMIP 2 model results over China, and obtained the largest cooling from the PMIP1 experiments with atmosphere GCM coupled with slab ocean model, whereas the least cooling is reproduced in the PMIP1 with prescribed SST using CLIMAP reconstructions (CLIMAP, 1981). The PMIP2 model experiments with fully coupled atmosphere–ocean GCM led to intermediate cooling between the two PMIP1 experiments. From Jiang et al. (2011), the annual-mean surface temperature change over Korea could be evaluated. Over Korea, PMIP1 with prescribed SST produces 5–6 C°, while PMIP1 with slab ocean model reproduces a larger cooling range, from 7.5 C° to 8.5 C°. In the PMIP2 case, the LGM surface cooling ranges from 5 to 6.5 C° over Korea. Overall, the combination of PMIP1 and PMIP2 indicates 5.5–6.5 C° cooling over Korea, which is slightly larger than the degree of cooling obtained in the PMIP3 experiments.

Table 2
Difference in surface air temperature (SAT) and precipitation between the LGM and pre-industrial simulations from multi-model average. Units are C° in SAT and mm day^{-1} in precipitation. Percent change in precipitation is shown in parentheses.

	DJF	MAM	JJA	SON	Annual
SAT	−9.70	−4.01	−2.69	−7.02	−5.85
Precipitation	−1.06 (−56)	−0.38 (−10)	0.44 (12)	−0.92 (−35)	−0.48 (−14)

3.2. Precipitation

The reduced surface temperature might limit the evaporation into the atmosphere and subsequently result in the reduction of precipitation. The LGM evaporation decreases over the Korean Peninsula according to PMIP simulations. Precipitation changes for a given region are jointly determined by large-scale water vapor advection, water vapor flux and its divergence, evapotranspiration, and water vapor content in the atmospheric column over the target region. Fig. 2 displays the geographic distribution of the change in precipitation in the LGM. Contour lines represent percent change. As would be expected from the reduction of surface temperature, precipitation overall decreases in the LGM over Korea. The largest reduction of precipitation in the LGM occurs in winter (Fig. 3a). For example, in COSMOS-ASO, precipitation decreases by more than 3 mm/day (80%) over the central part of the Korean Peninsula. The MIROC model also reproduced the substantial decrease in precipitation in the southeastern part of Korea by more than 1.2 mm/day (about 70%). Even though the reduction amount of precipitation is small, the percent change is large in the MRI GCM. In the MPI model, the least reduction of precipitation occurs in western and southern part of the peninsula by less than 0.3 mm/day (less than 20%). Overall, in winter precipitation reduction quantity is larger in the southeastern part of Korea by more than 1.2 mm/day, but percent change is larger in the central part of the Korean Peninsula, by about 50%.

In spring, the largest reduction in precipitation is reproduced in the IPSL model in the southernmost part of the Korean Peninsula by more than 1.2 mm/day (more than 20% reduction). The second largest reduction is found in the COSMOS model by more than 0.9 mm/day, which is more than 20% reduction. In contrast to the overall reduction in precipitation in spring, the precipitation substantially increased in the FGOALS model in the LGM simulation, especially in the northern part of North Korea, by more than 0.9 mm/day (50%) and western South Korea by more than 0.6 mm/day (20%). In CNRM, MIROC, MPI, and MRI GCMs, precipitation slightly increases in some parts of Korea, but the amount is quite small. Overall, in spring, precipitation decreases by 0.3–0.6 mm/day in South Korea (more than 10% reduction) and by less than 0.3 mm/day in North Korea (less than 10% reduction).

In contrast to the overall reduction in precipitation in winter and spring seasons over Korea, in summer, precipitation increases in almost the entire Korean Peninsula. In summer, the largest increase in LGM precipitation is reproduced in the MIROC model, especially in the southwestern corner of Korea, where precipitation increases by more than 2 mm/day (more than 70%). A moderate degree of precipitation increase is also found in the rest models except for the IPSL model, where precipitation overall decreases. Almost all models show more increase in precipitation in the western part of South Korea and eastern part of North Korea. Overall, in the LGM summer, precipitation increases and the maximum increase is found in the western part of South Korea, where precipitation increases by more than 0.6 mm/day (more than 20%).

In autumn, precipitation decreases in the LGM. The largest reduction of precipitation occurs in the COSMOS and MIROC GCMs in the southeastern part of South Korea, by more than 1.8 mm/day. However, the reduction amount of precipitation is not consistent with percent change, because in the COSMOS model the larger reduction in precipitation occurs in the western half of South Korea by more than 60%. In the MIROC model, precipitation decreases more in the central part (by more than 40%) of the Korean Peninsula than in the southeastern corner. In FGOALS and CNRM,

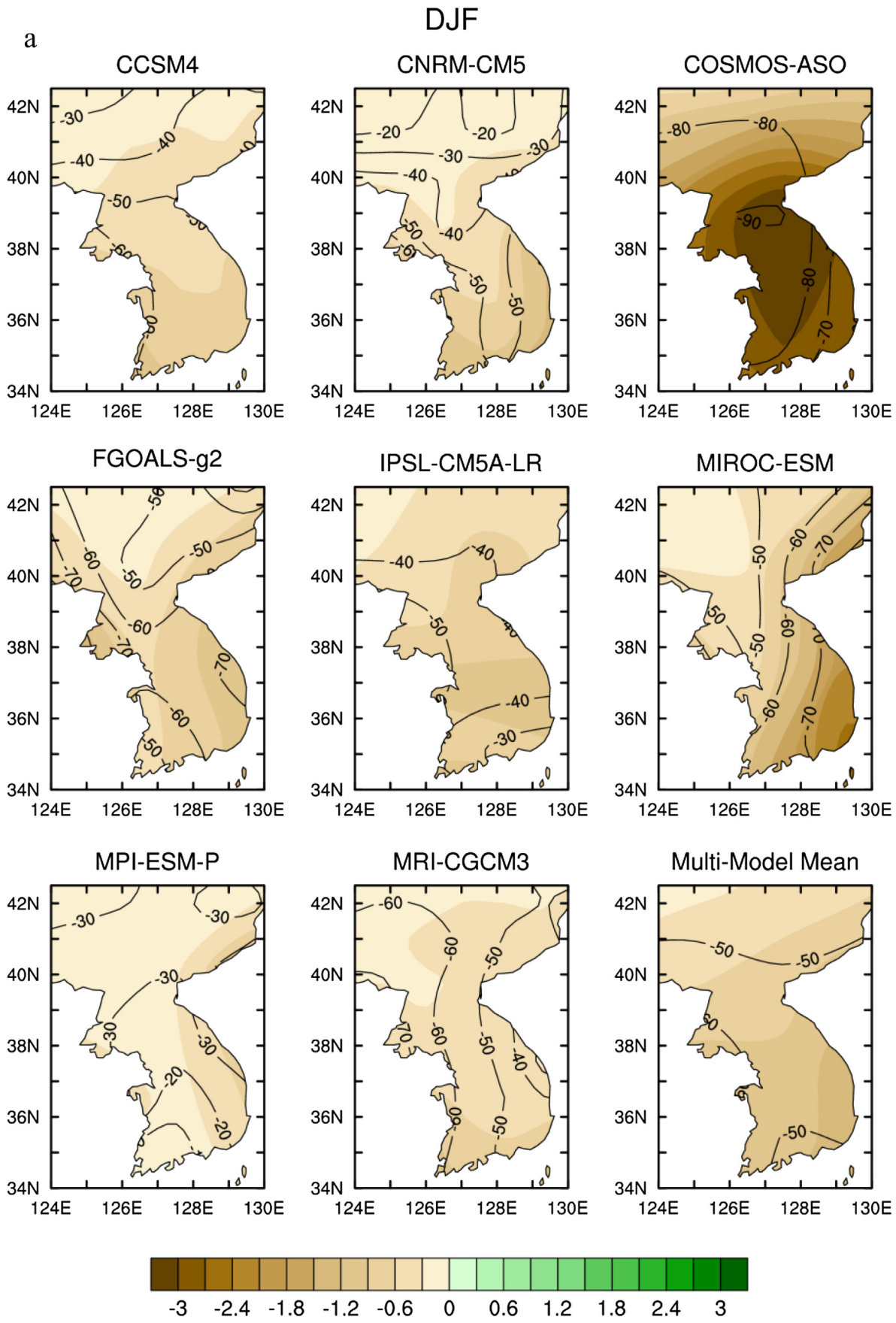

Fig. 3. Geographic distribution of the change in precipitation between the LGM and pre-industrial simulations for a) DJF, b) MAM, c) JJA, d) SON, e) annual-mean. Units are in mm day^{-1} for precipitation amount in shading and % for contour lines.

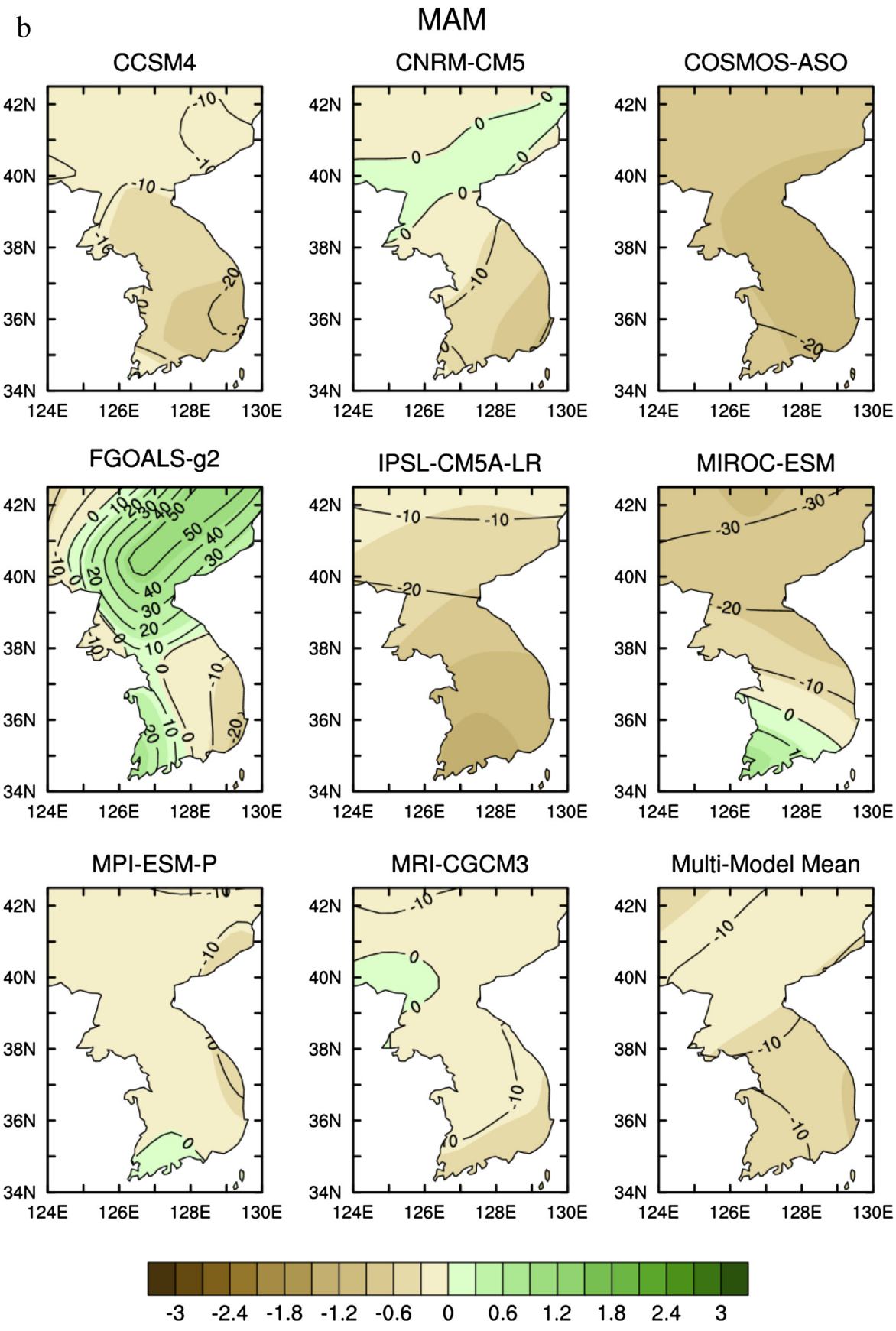

Fig. 3. (*continued*).

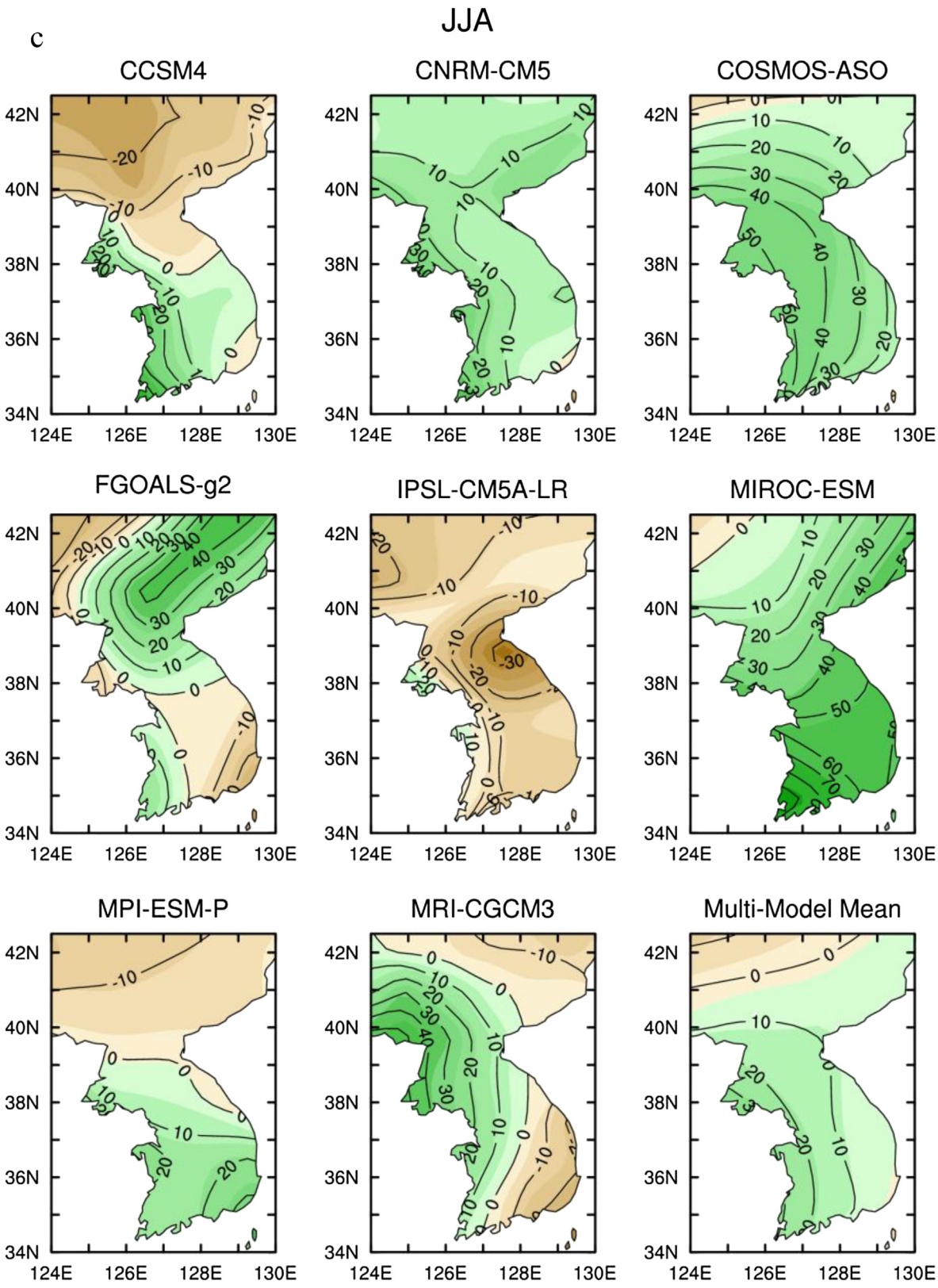

Fig. 3. (*continued*).

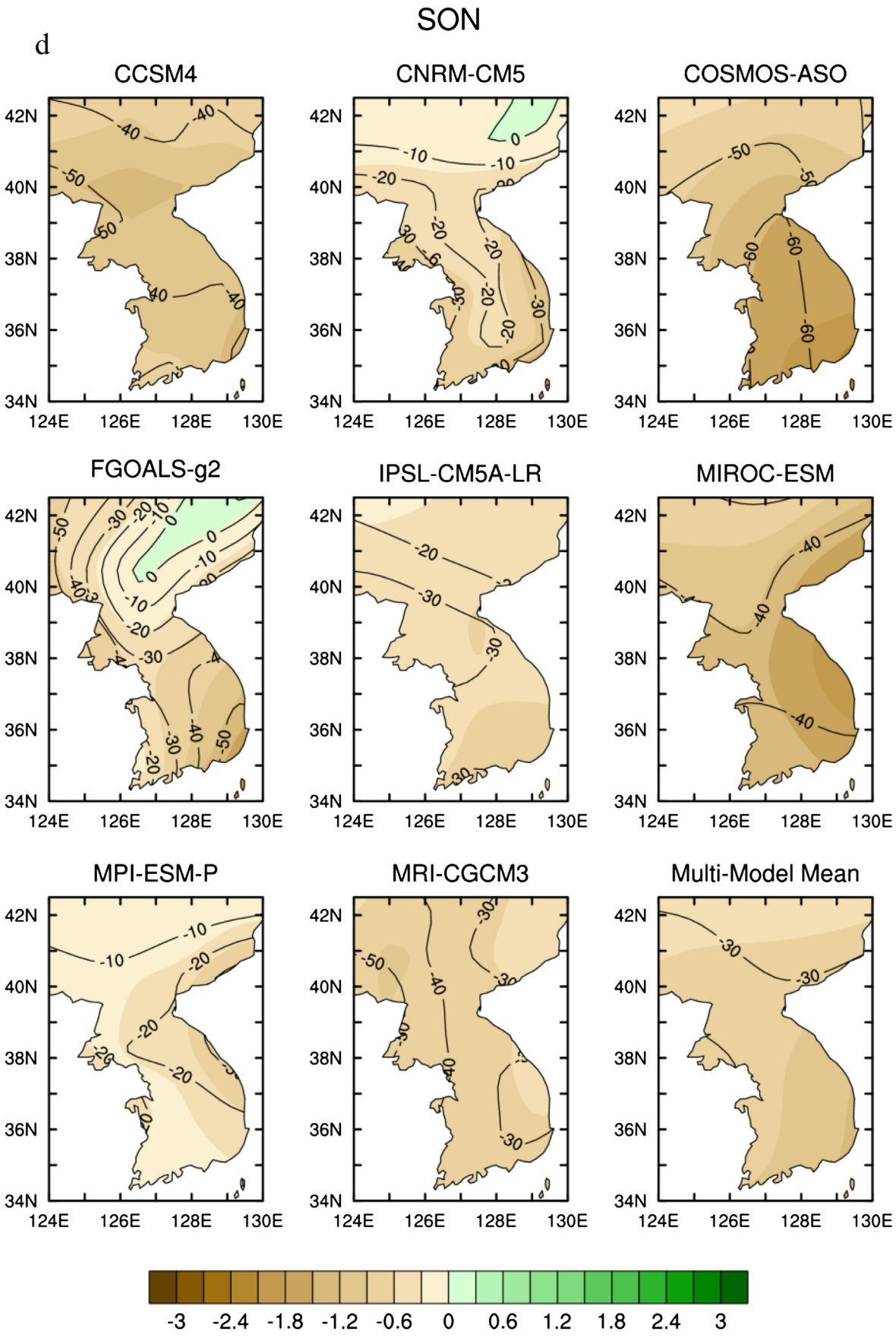

Fig. 3. (*continued*).

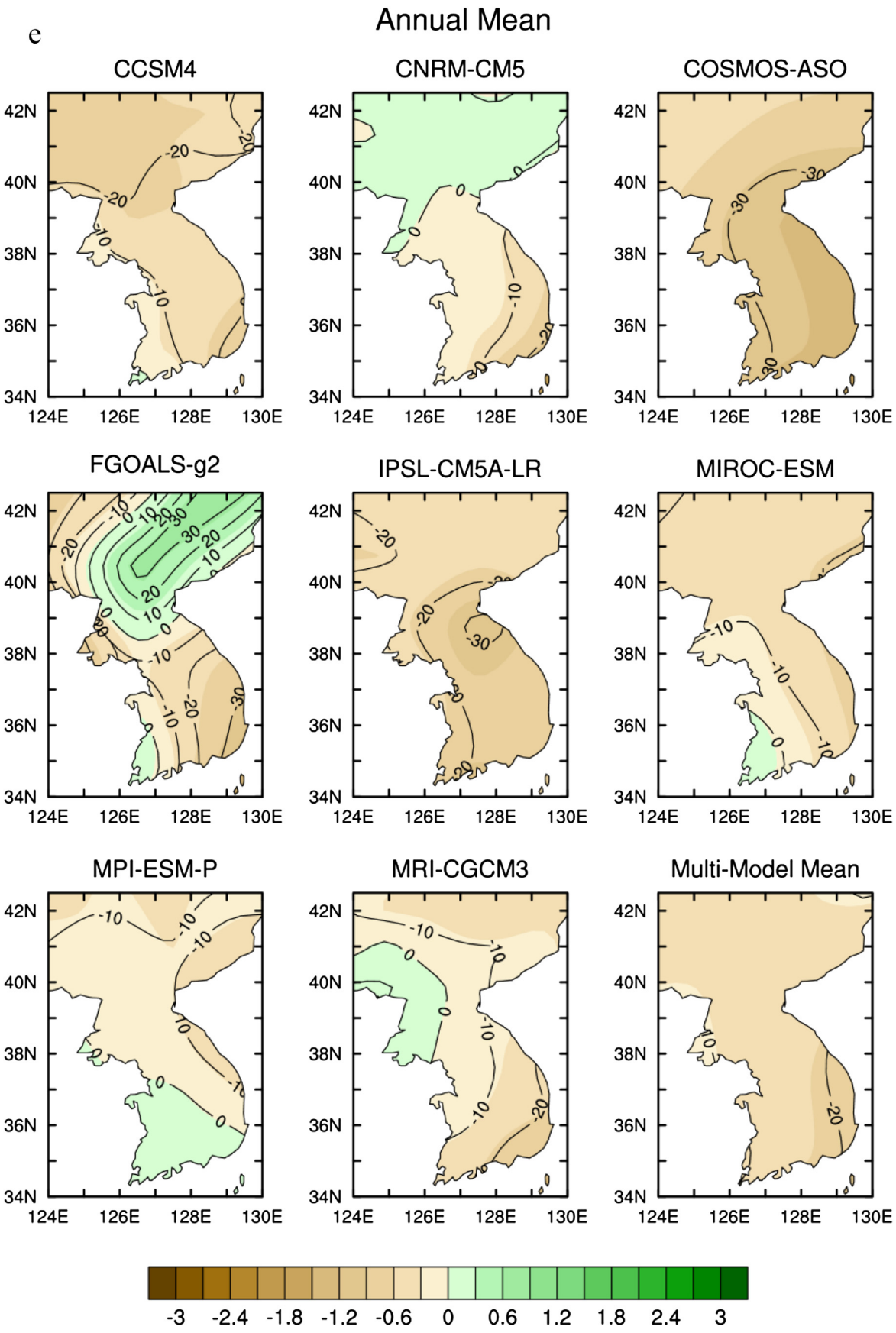

Fig. 3. (*continued*).

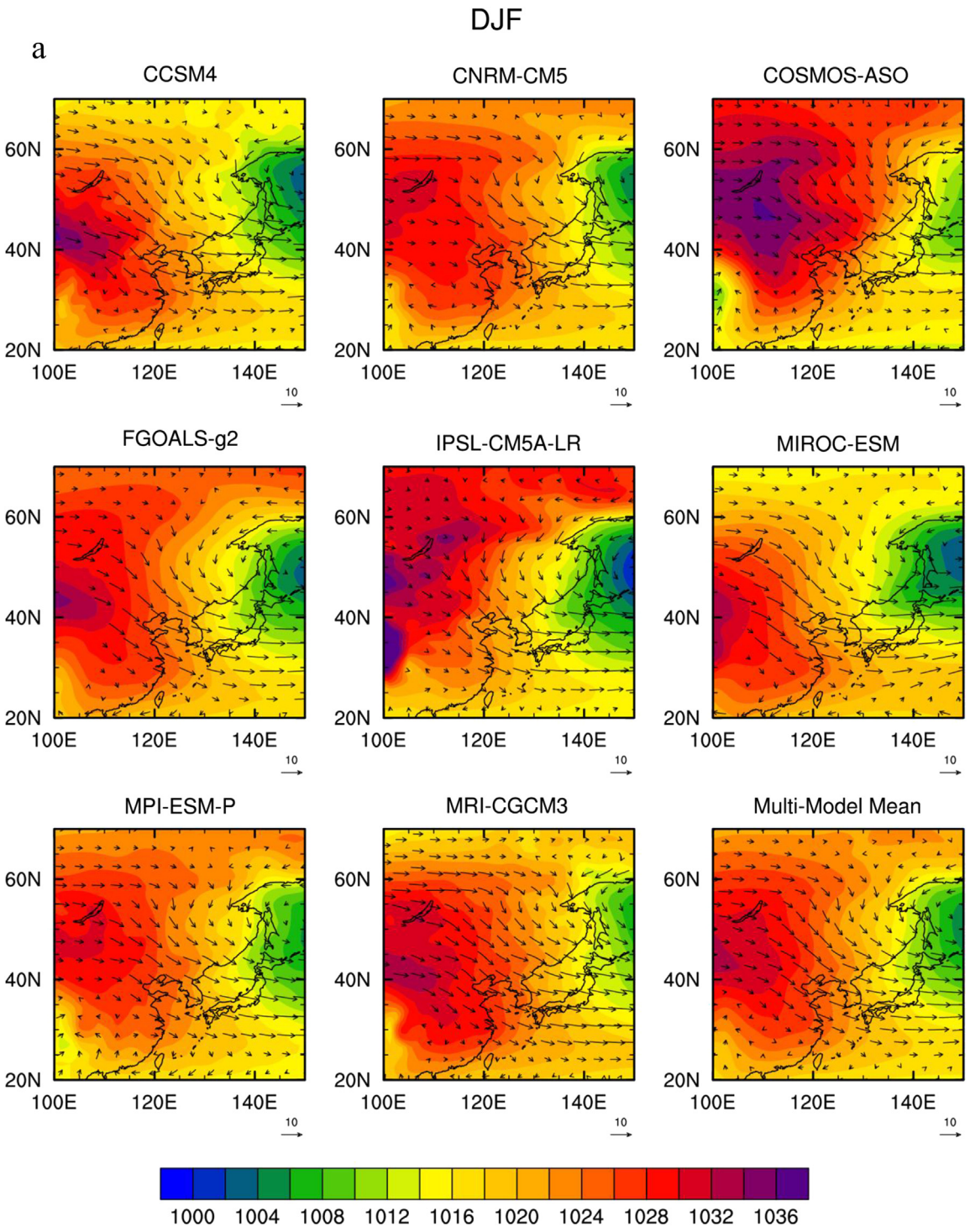

Fig. 4. Geographic distribution of the seasonal-mean wind vectors with sea level pressure magnitude (color) for pre-industrial simulation at the 850-hPa level for a) DJF, b) MAM, c) JJA, d) SON, e) annual-mean. The wind vector magnitude in the box.

precipitation increases slightly in northeastern Korea, but the increase is relatively small. Overall, in LGM autumn, precipitation reduction ranges from 0.6 to 1.2 mm/day (more than 30% reduction), and more precipitation decrease is found towards the south, with the maximum reduction in the southeastern part by more than 1.2 mm/day.

The largest reduction of annual-mean precipitation is reproduced in the COSMOS-ASO model by more than 1.2 mm/day in the southeastern part of Korea, about a 30% reduction from the PI value. In the FGOALS model, precipitation appears to increase by more than 0.6 mm/day (about 30%) in the LGM in the northern part of the peninsula. Overall, in the LGM, annual mean precipitation reduction ranges from 0.3 to 0.6 mm/day (10–20%) and precipitation reductions are larger in the southeastern part of the Korean Peninsula.

Regional mean precipitation is substantially reduced in winter of the LGM. As in the SAT change, the largest precipitation decrease by more than 3 mm/day is reproduced in the COSMOS model,

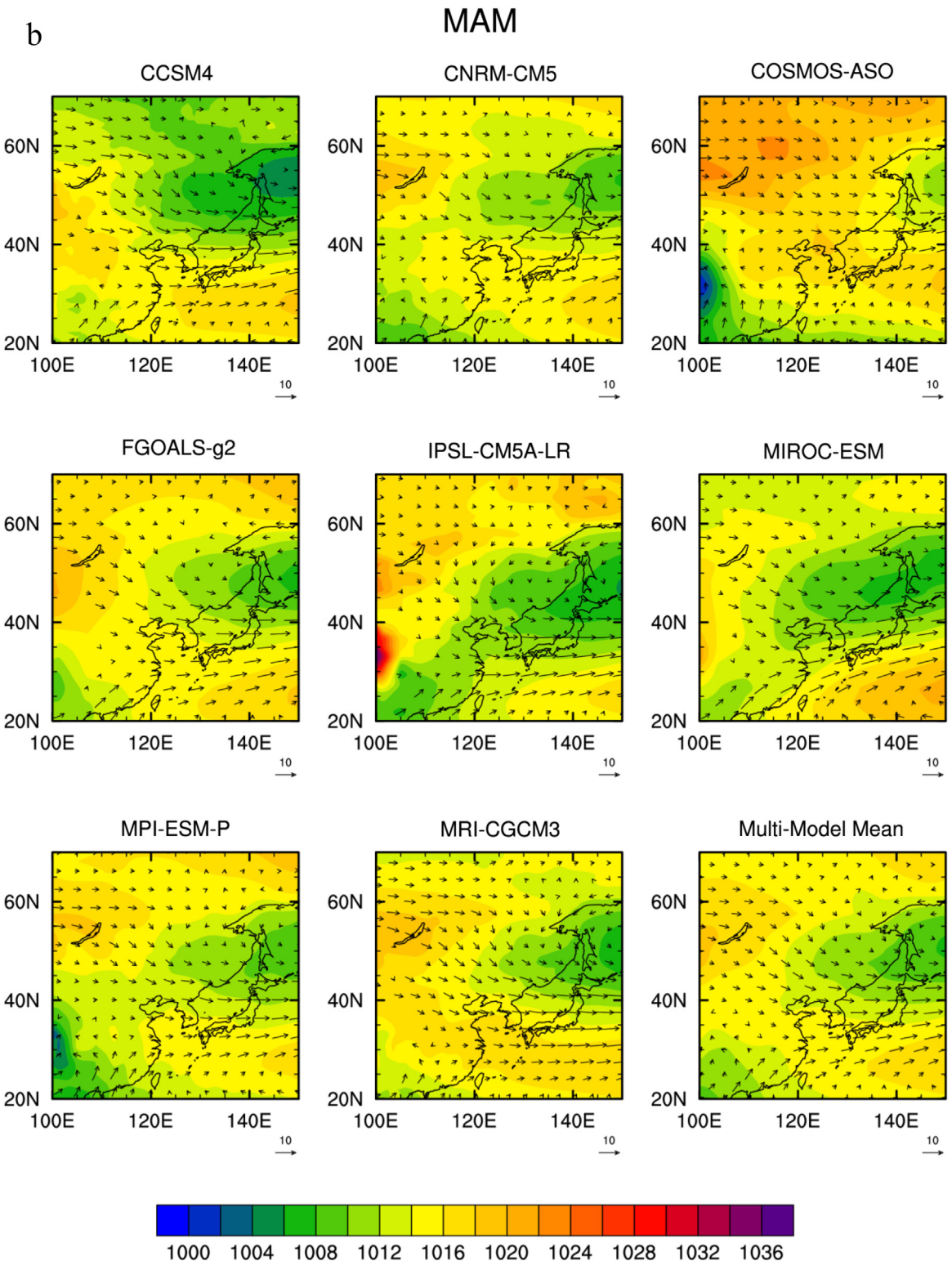

Fig. 4. (*continued*).

whereas the least precipitation change over Kore occurs in the MPI model. Multi-model mean precipitation reduction is 1.06 mm/day, 56% reduction (Table 2). In spring, precipitation change is very little with a slight reduction, except for the FGOALS where precipitation increases slightly in the LGM spring. Spring precipitation reduction is 0.38 mm/day (10%) in the LGM. In summer, precipitation appears to increase in most models with multi-model mean of 0.44 mm/day (12%), except for the IPSL model, where precipitation decreases by more than 1 mm/day in the LGM. In autumn, precipitation decreases in all models with multi-model averaged of −0.92 mm/day, 35% reduction. Overall, in the LGM over Korea, annual-mean precipitation decreases by 0.48 mm/day, 14% reduction.

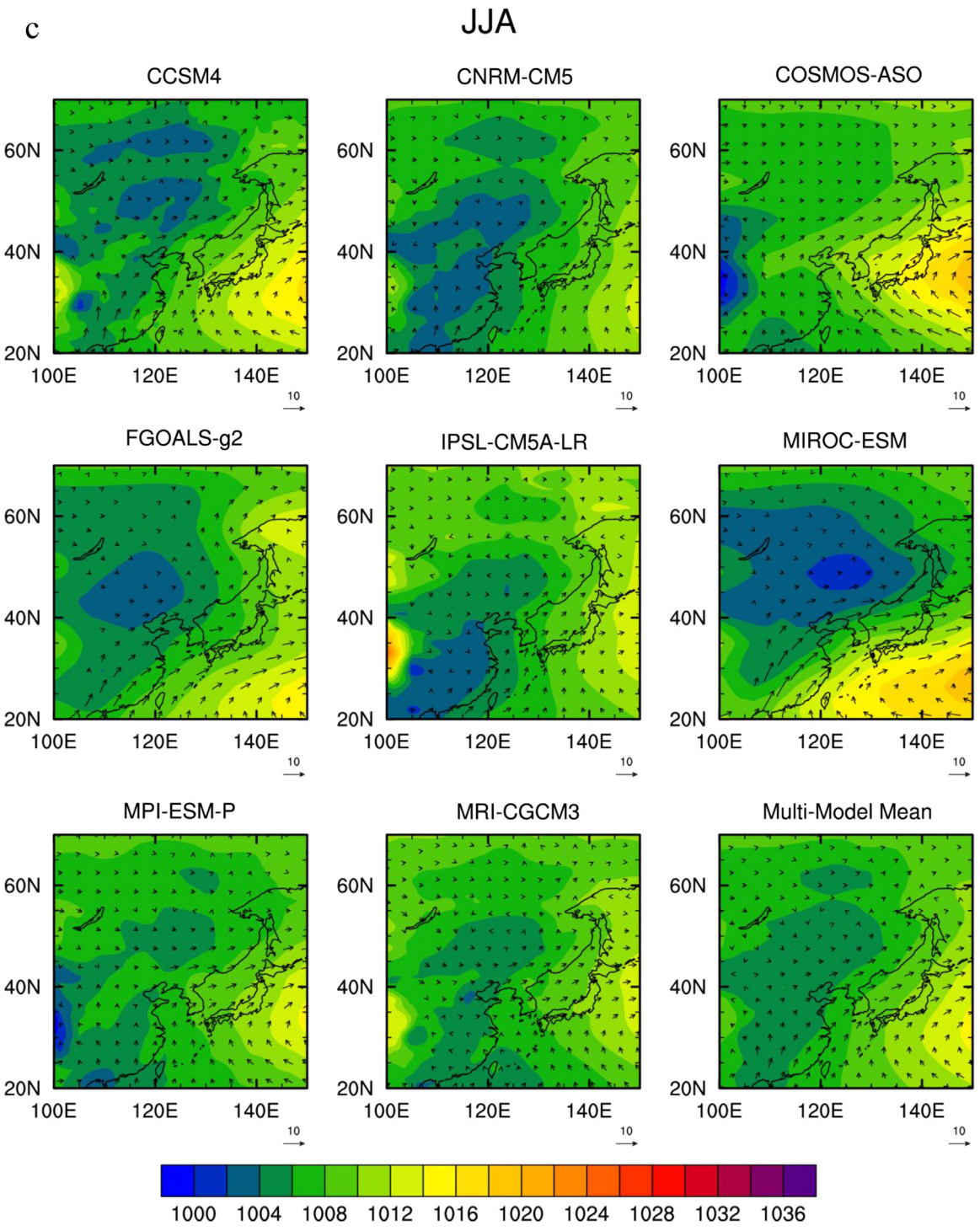

Fig. 4. (*continued*).

In the previous PMIP simulations, precipitation decreases over China and Korea. Jiang et al. (2011) show that the annual mean precipitation decreases by 25% in the northern part and by 40% over southern and southeastern Korea in the PMIP1 with prescribed SST case. On the other hand, in the AGCM coupled with slab ocean model experiment, the precipitation decrease is much less than the prescribed case in the LGM ranging from 10 to 17% over Korea. In the PMIP2 simulations, precipitation decreases from 15% to 20% over Korea. Overall, the PMIP1 with slab ocean experiments gives the closest change in precipitation to the PMIP3 results. The PMIP2 results are also within error ranges.

3.3. Low level winds

The Korean Peninsula is located between the Eurasian continent and North Pacific Ocean. The surface temperature of the Eurasian continent is very sensitive to changes in the diabatic heating field, whereas the North Pacific Ocean is relatively stable to a change in

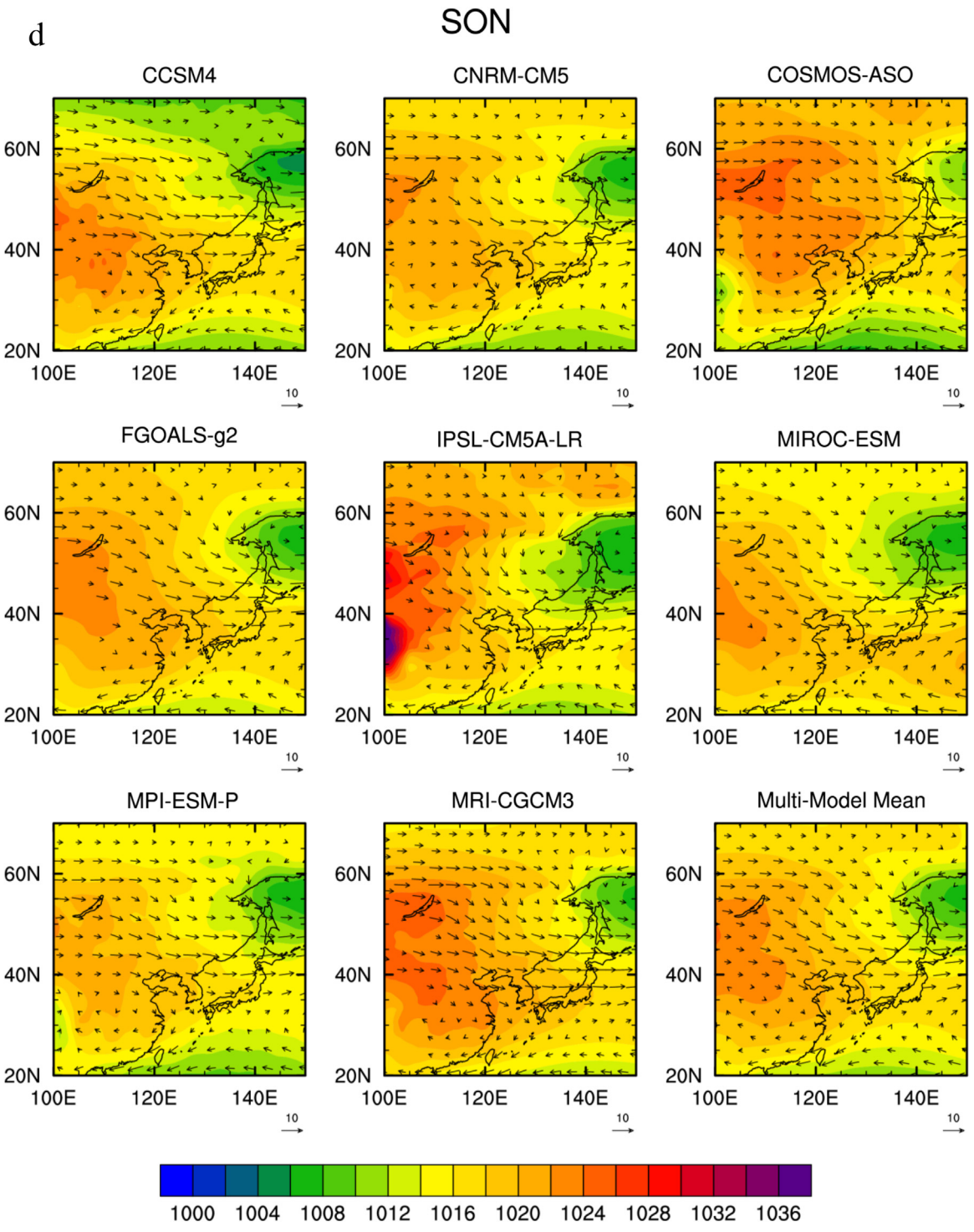

Fig. 4. (*continued*).

external heating because the ocean has much larger heat capacity than the land. Associated with this special geographic setting, the Korean Peninsula is strongly influenced by the seasonally varying land-sea thermal contrasts such as the Asian winter and summer monsoons.

In winter, because of the reduction in radiative heating and accumulation of snow over the Asian continent, extreme surface cooling occurs, especially over Mongolia and southern Siberia, and high pressure develops (Fig. 4a). All models capture the high pressure feature fairly well with sea level pressure by more than 1030 hPa. The high pressure developed over Mongolia and Southern Siberia leads to the anticyclonic circulation over central Asia, while in the Northwestern Pacific, cyclonic winds are reproduced associated with the low pressure. From this pressure distribution, the northwesterly winds are predominant over Korea in winter and this feature is well captured in all models used in the analysis. In spring, the high pressure over the Asian continent is still present, although its magnitude becomes substantially weaker (Fig. 4b).

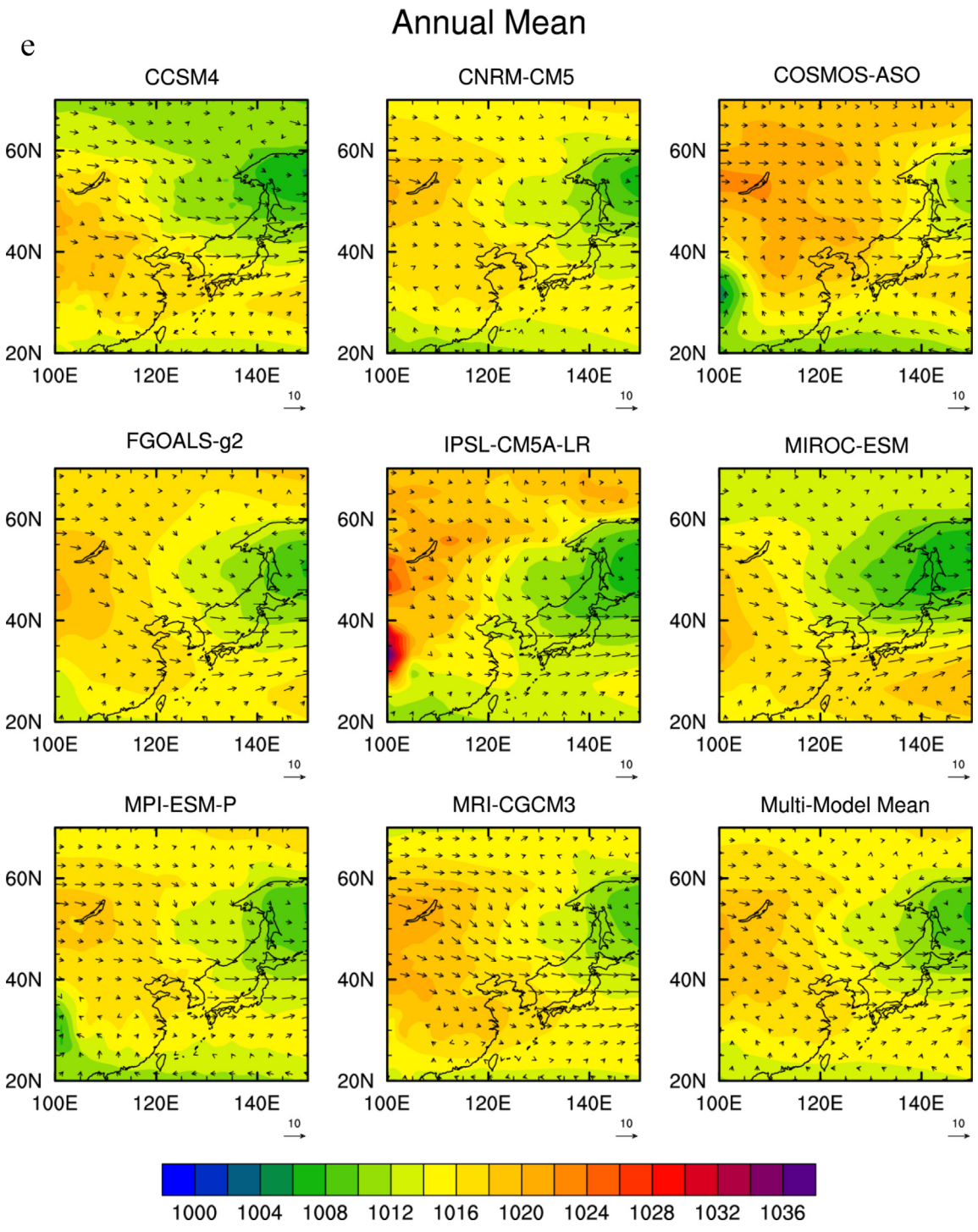

Fig. 4. (*continued*).

While in the North Pacific surface pressure is becoming stronger with anticyclonic circulation, in the northern North Pacific cyclonic circulation develops. This results in the predominant westerly wind pattern over Korea in spring.

Towards summer, the increasing shortwave radiation heats the Asian continent and results in the low pressure relative to the North Pacific, where a relatively high pressure, referred to as western North Pacific High, develops (Fig. 4c). The western North Pacific High leads to the southwesterly winds over Korea, bringing moisture and heat from low latitudes. In autumn, with the shortage of short wave radiative heat flux, the high pressure over the Asian continent becomes stronger, while the cyclonic pressure is maintained over the northern North Pacific, resulting in northwesterly and westerly winds over Korea.

In the LGM simulations, most models show weakening of low-level north-westerly winds in winter, leading to anonymously strong southerly and south-easterly winds (Fig. 5a). In high northern latitudes, in the LGM, sea level pressure is larger than to the south, and this pattern provides easterly wind anomalies. However, FGOALS and MIROC show enhanced surface winds with northwesterly anomaly. Overall, in winter, the southwesterly wind anomaly in the southern part of Korea and northwesterly wind

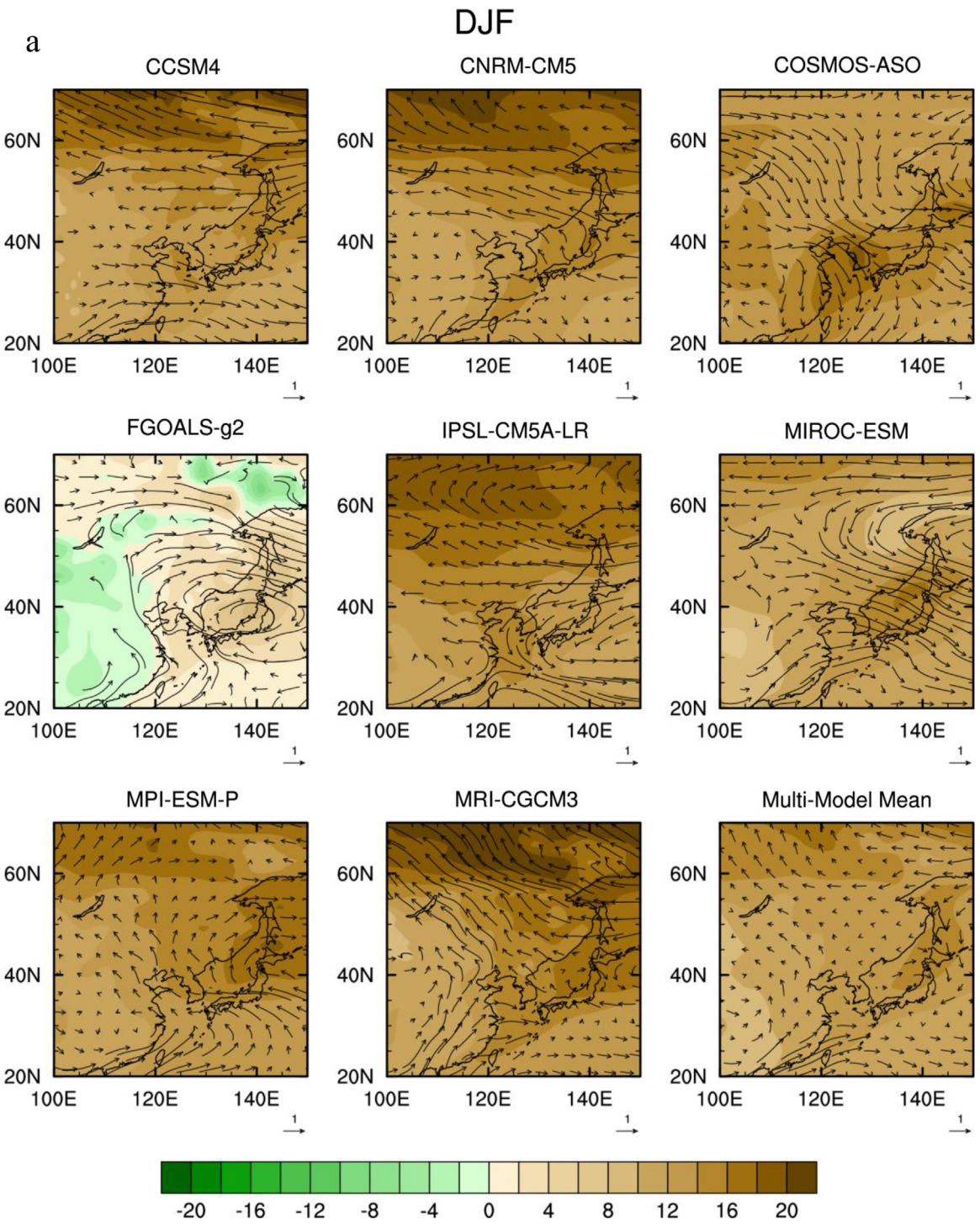

Fig. 5. Geographic distribution of the change in winds between the LGM and pre-industrial simulations for a) DJF, b) MAM, c) JJA, d) SON, e) annual-mean.

anomaly in the northern part of Korea part are predominant, consistent with previous PMIP simulation results (Jiang and Lang, 2010). This indicates that the east Asia winter monsoon is enhanced in the LGM. The change is relatively small because of model to model variations.

In spring, the increase in pressure occurs in high latitudes as well as in low latitudes (Fig. 5b). The increase in pressure in high latitudes leads to the easterly wind anomaly, whereas in low latitudes the increase in pressure results in a westerly wind anomaly. In the LGM spring, anticlockwise wind anomalies are reproduced over Korea.

In summer, pressure increases almost everywhere, especially in high latitudes and over the Asian continent. The increase in pressure over high latitudes again leads to easterly wind component, while in low latitudes it results in westerly winds. Eventually, cyclonic wind anomalies are developed. There is one exception. In the FGOALS model, in the LGM sea level pressure decreases in the south of Korea and owing to this pressure difference easterly wind

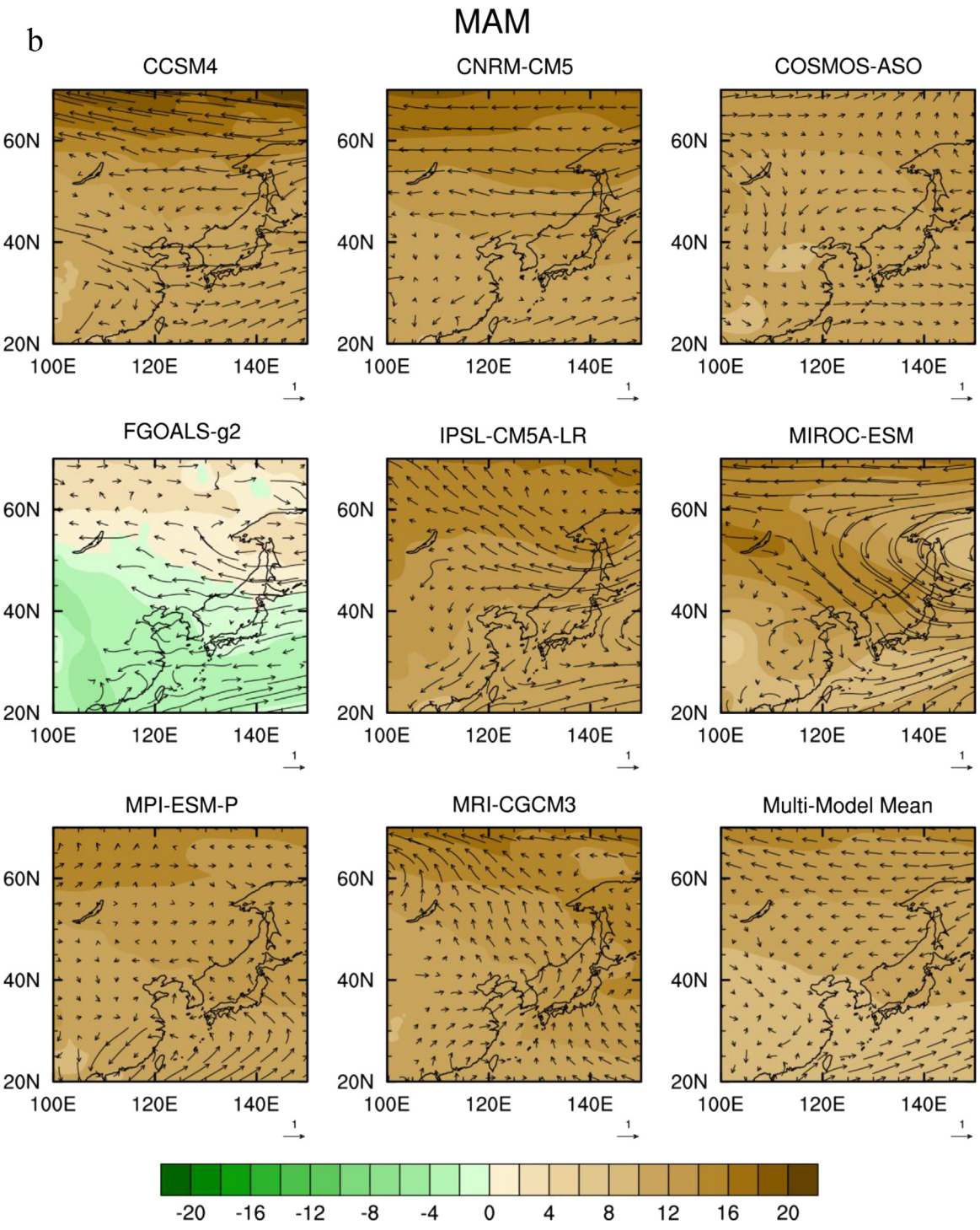

Fig. 5. (*continued*).

anomaly is predominant. The cyclonic wind anomalies in summer are consistent with previous PMIP simulations (Jiang and Lang, 2010), indicating the east Asian summer monsoon was weaker in the LGM. In autumn, a similar feature is repeated with the increase in pressure over high and low latitudes, with anticlockwise circulation.

The change in surface winds is closely linked to the change in the baroclinicity (i.e. meridional temperature gradient). Fig. 6 displays the change in meridional temperature gradient at 850 hPa between the PI and LGM. In winter, most models show the increase in baroclinicity in the south of Japan, connected to the interior of the Asian continent, while in the north of Japan, the baroclinicity decreases. The largest increase in baroclinicity at the south of Japan is related to the marked reduction of temperature over the Korean Peninsula and East/Japan Sea relative to the change in temperature in the low latitudes. On the other hand, the decrease in baroclinicity in northern Japan is related to the relatively lesser temperature reduction in high northern latitudes. The location of maximum

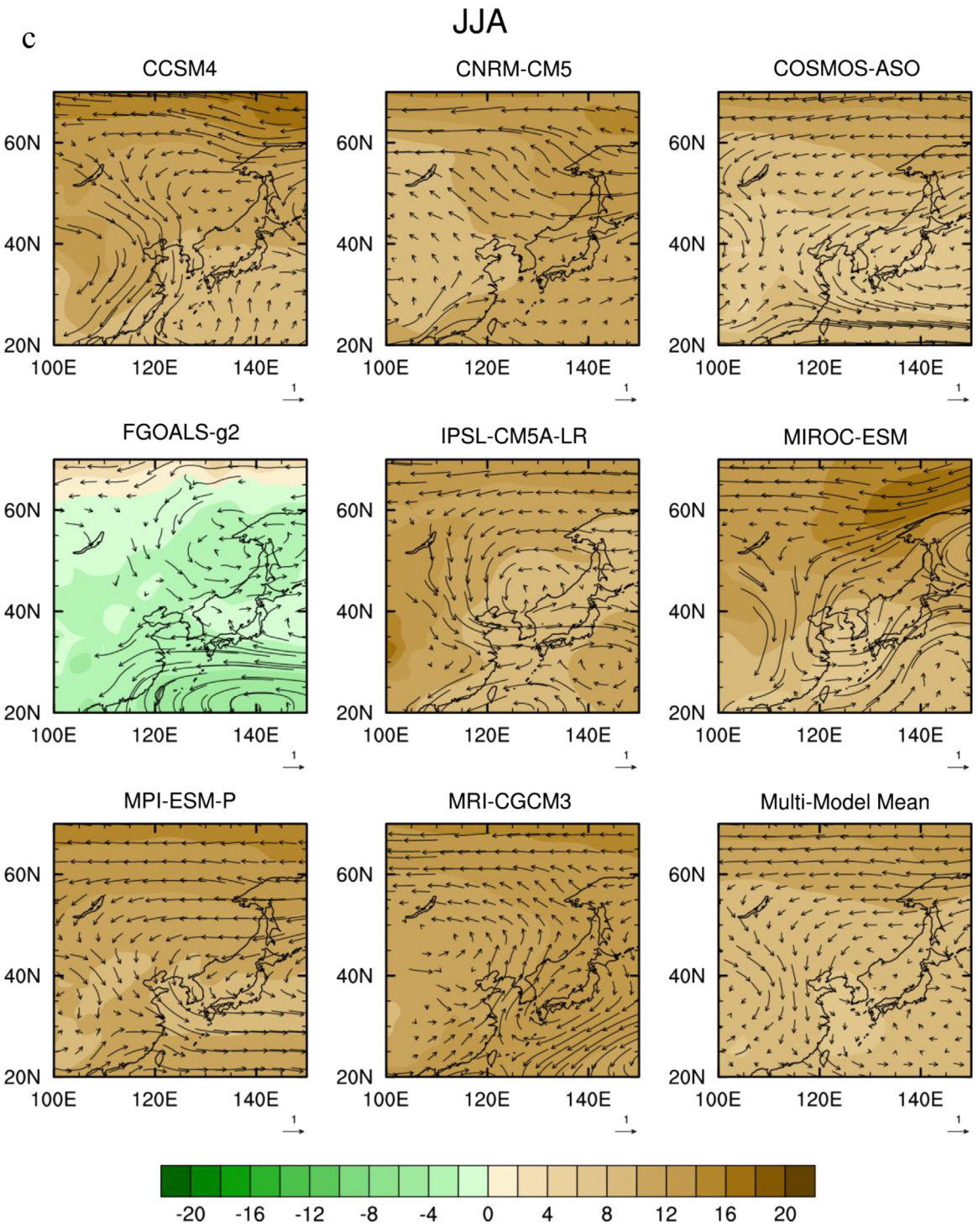

Fig. 5. (*continued*).

westerly wind anomaly in the southern Korean Peninsula is consistent with the area of the largest increase in baroclinicity with larger meridional pressure gradient, whereas the easterly wind anomaly in northern high latitudes are associated with the reduction in baroclinicity. In spring, the change in baroclinicity is overall similar to that of winter, but with lesser degree of change. This is related to the lesser degree of temperature change in spring than in winter. In summer, the location of the maximum increase in baroclinicity is displaced to the north slightly, but with generally similar features with other seasons. In autumn, the baroclinicity change is overall similar to other seasons.

Overall, in the LGM, the decrease in surface temperature leads to the increase in surface pressure everywhere, and the larger increase is found in high latitudes. The increase in surface pressure and reduction in baroclinicity in high latitudes results in the easterly wind anomaly, while in the south the increase in pressure and

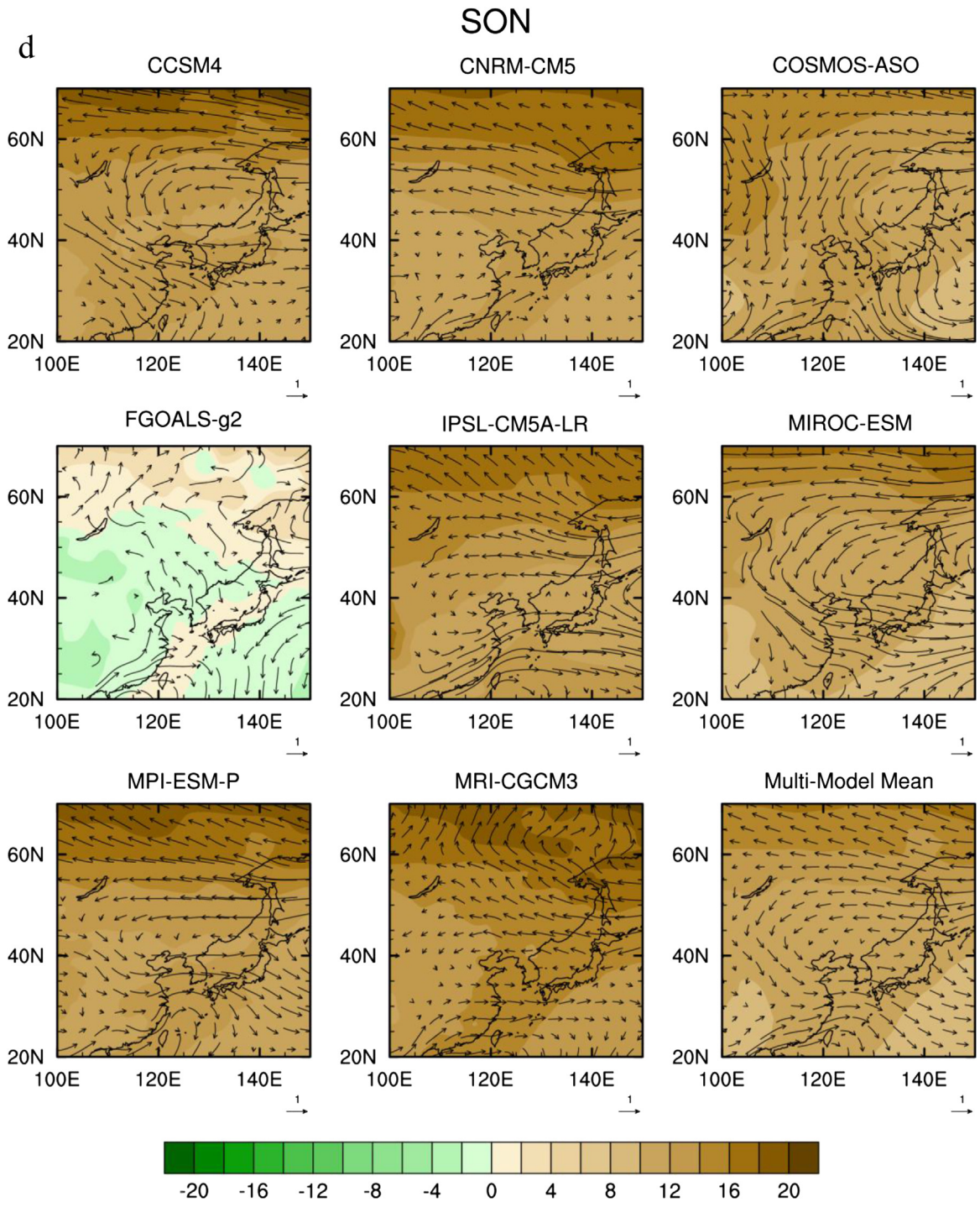

Fig. 5. (*continued*).

baroclinicity leads to the westerly wind anomaly. Due to this anomalous wind pattern, there are predominant cyclonic wind anomalies over Korea in the LGM.

4. Comparison to LGM climate reconstruction by proxy data

There are few studies on the LGM climate reconstruction over Korea. Using pollen analysis from the Quaternary sediment cores sampled in Hanam City east of Seoul, Korea, Yi et al. (2008) reconstructed paleo climate and paleo vegetation, and found subalpine coniferous consisting of spruce and pine together with xerophytic herbs during the last glacial period (21.6 ka BP~14.9 ka BP), indicating cold and dry climate. However, rainfall might have varied in the Hanam City area, with possible increase in rainfall between 19.2 ka BP and 17.7 ka BP with sudden appearance of colonial green algae. Between 26.1 ka BP and 20.1 ka BP, the Hanam pollen assemblages are dominated by conifers and cold-tolerant deciduous broadleaved type vegetation. Principal taxa are similar to the subalpine forest, indicating cold and dry conditions. From 22.5 ka BP to 20.5 ka BP, cold and wet

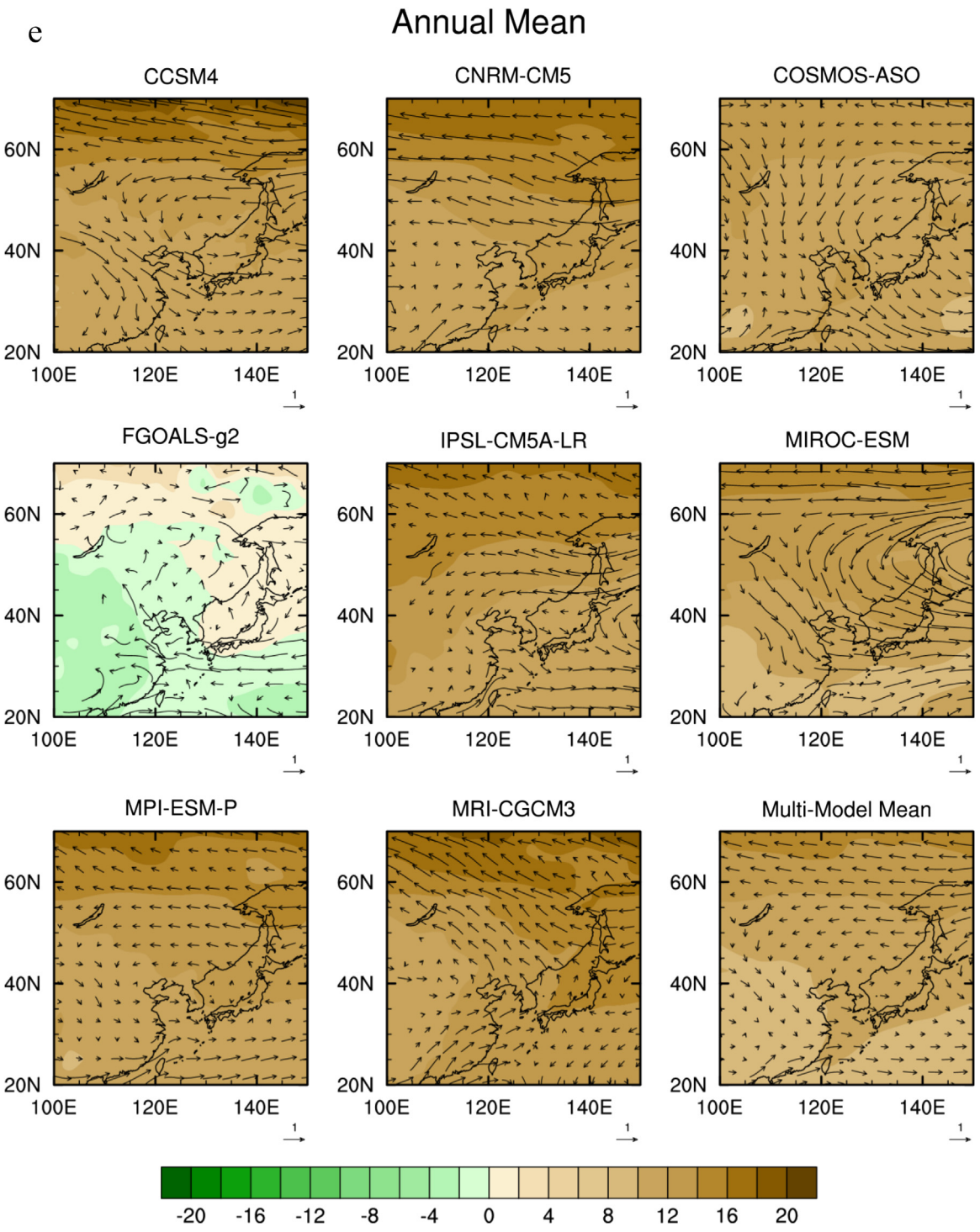

Fig. 5. (*continued*).

conditions were reconstructed with low aridity index, with conifers and temperate deciduous broadleaved mixed forests (Yi and Kim, 2010). From 22.5 ka BP to 20.5 ka BP, climate changed into colder and drier conditions with an abundance of *Picea* and *Betula* associated with high aridity index and subalpine conifers.

By analyzing plant types using the sediment sample from Cheollipo, on the Taean Peninsula, western coast, Lim et al. (2010) found a yellowish MIS 2 layer, indicating dry-land environment with low vegetation cover. Lim et al. (2010) analyzed total organic carbon content and estimated C_4 plant abundance, and found during the LGM C_4 plant content was about 20%, which is substantially lower than the mid-Holocene (about 40%). The lower C_4 abundance in the LGM indicates a lower surface temperature than the mid-Holocene, due to an intensified winter monsoon and SST decrease in the East Sea owing to limited influx of the Tsushima warm current because of lowered sea level.

The colder and drier climatic conditions over Hanam area and drier climate in the eastern coast of Korea in the LGM

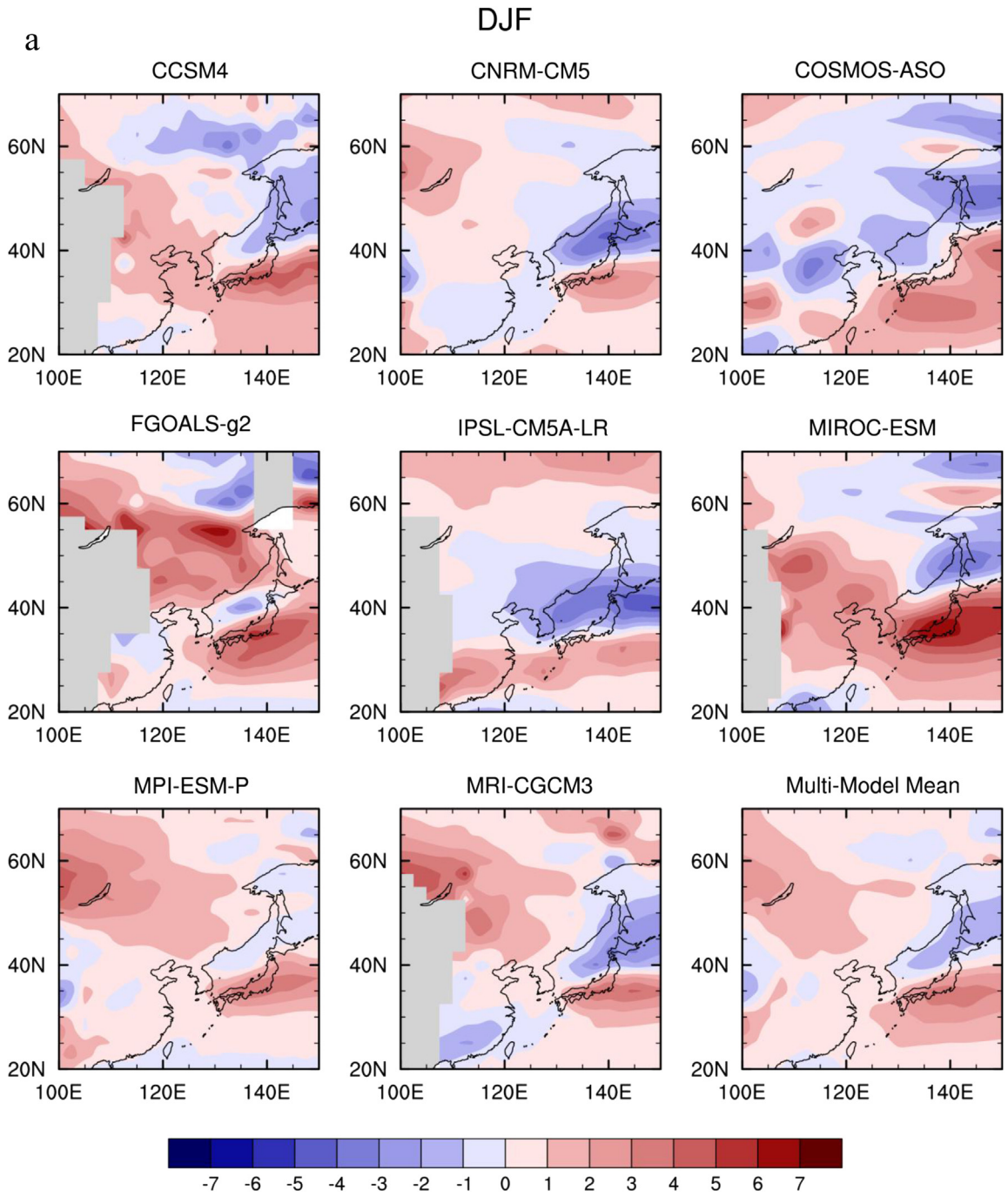

Fig. 6. Geographic distribution of the change in meridional temperature gradient at 850 hPa between the LGM and pre-industrial simulations for a) DJF, b) MAM, c) JJA, d) SON, e) annual-mean. Unit is 10^{-6} km/m.

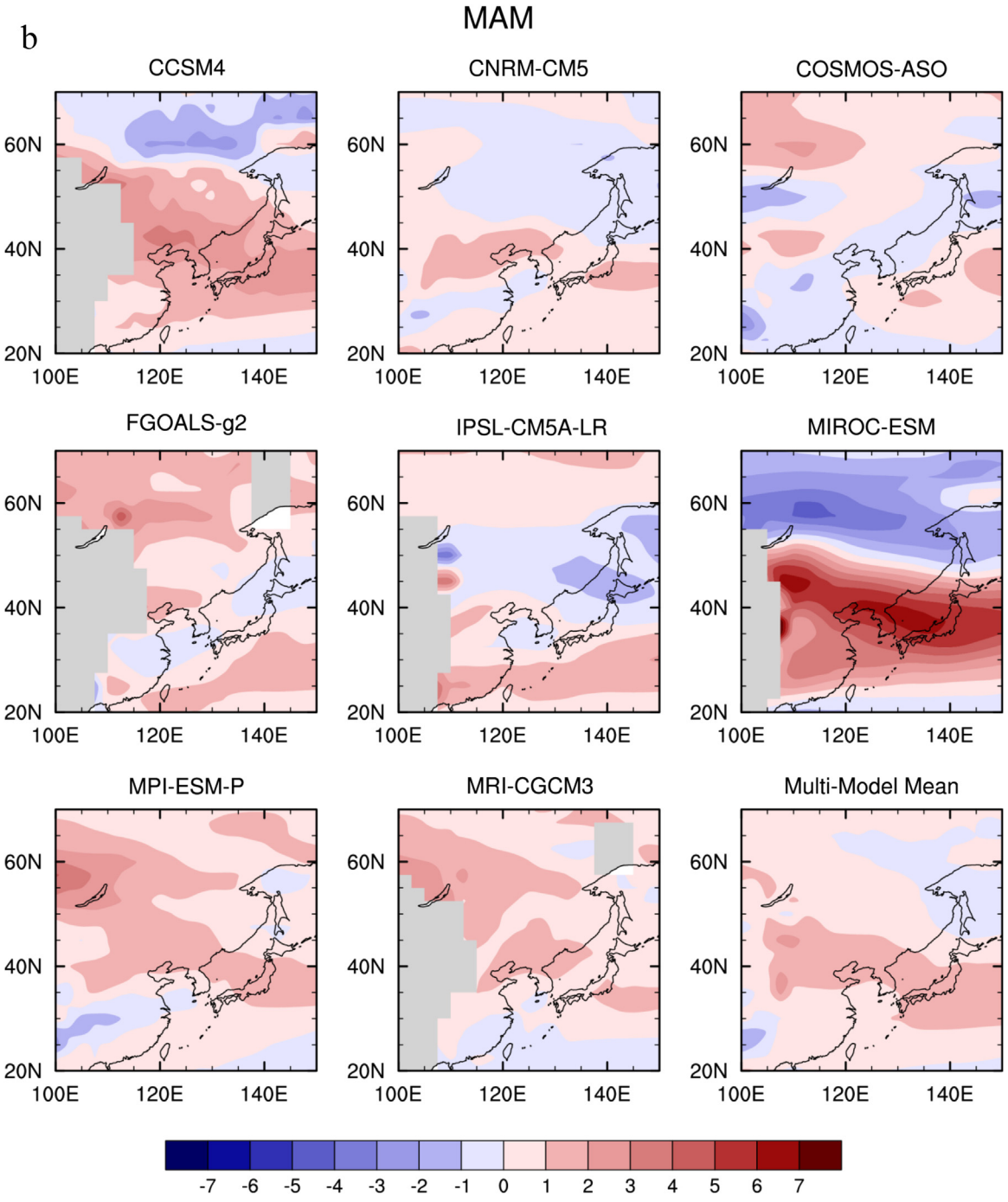

Fig. 6. (*continued*).

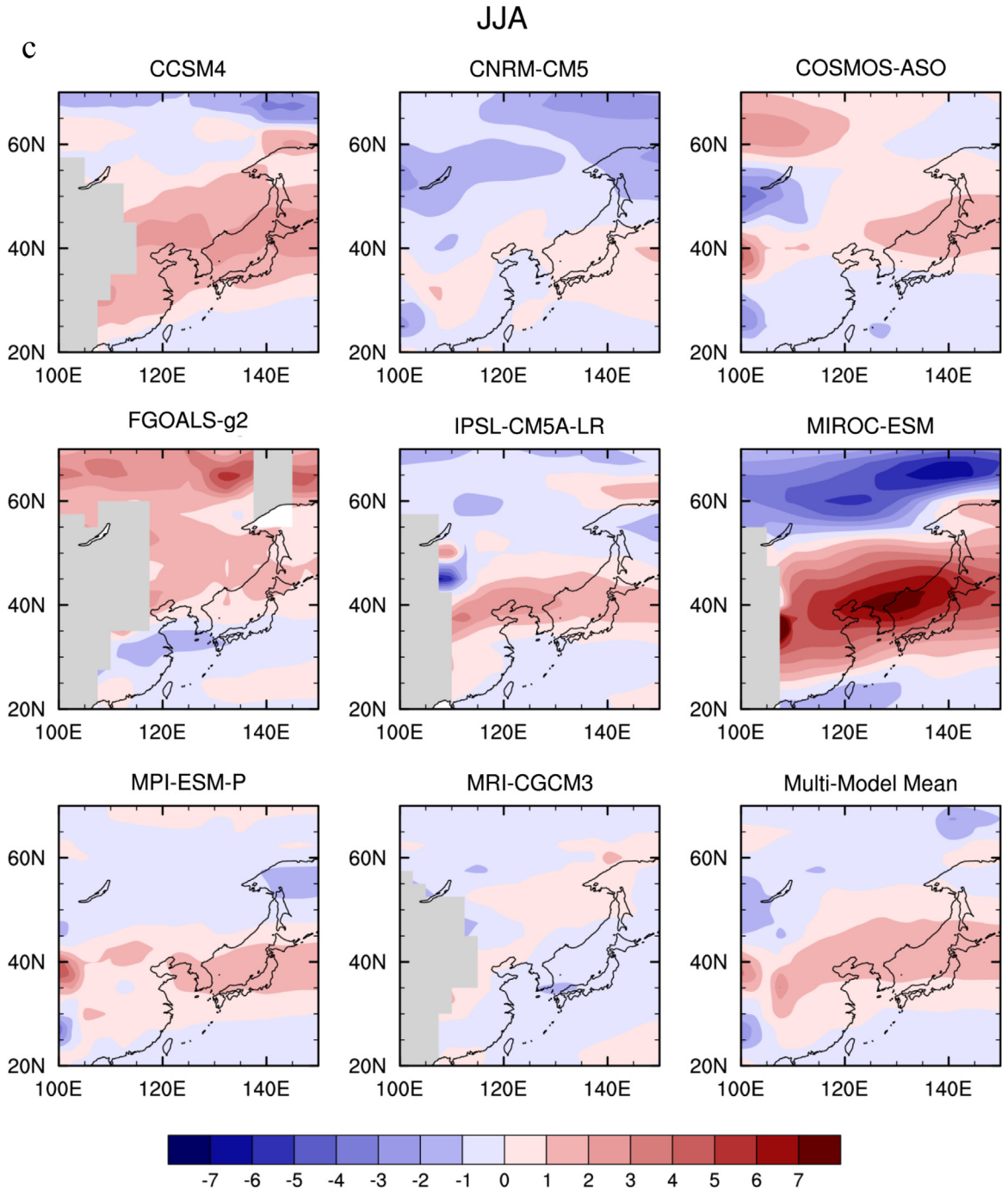

Fig. 6. (*continued*).

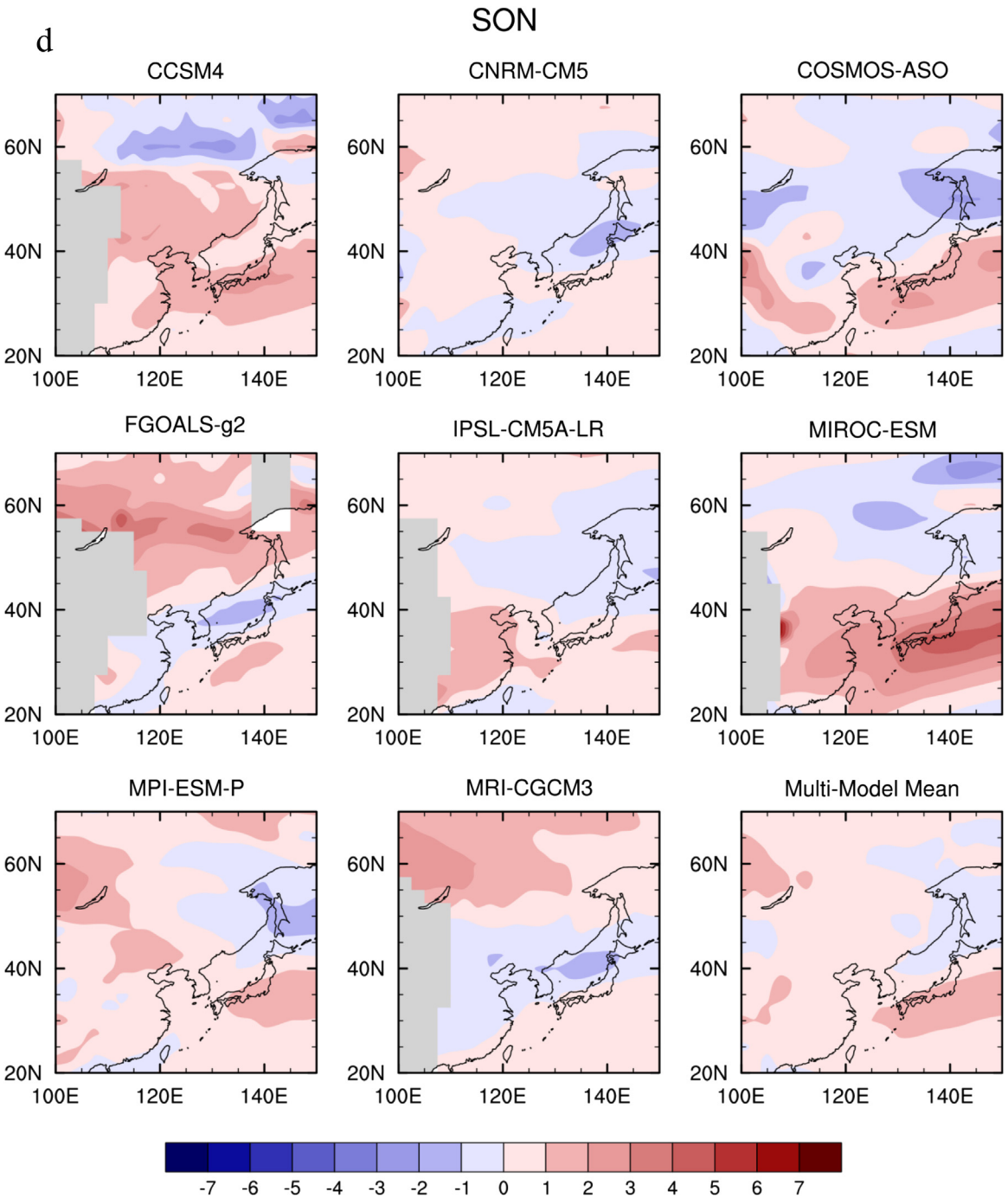

Fig. 6. (*continued*).

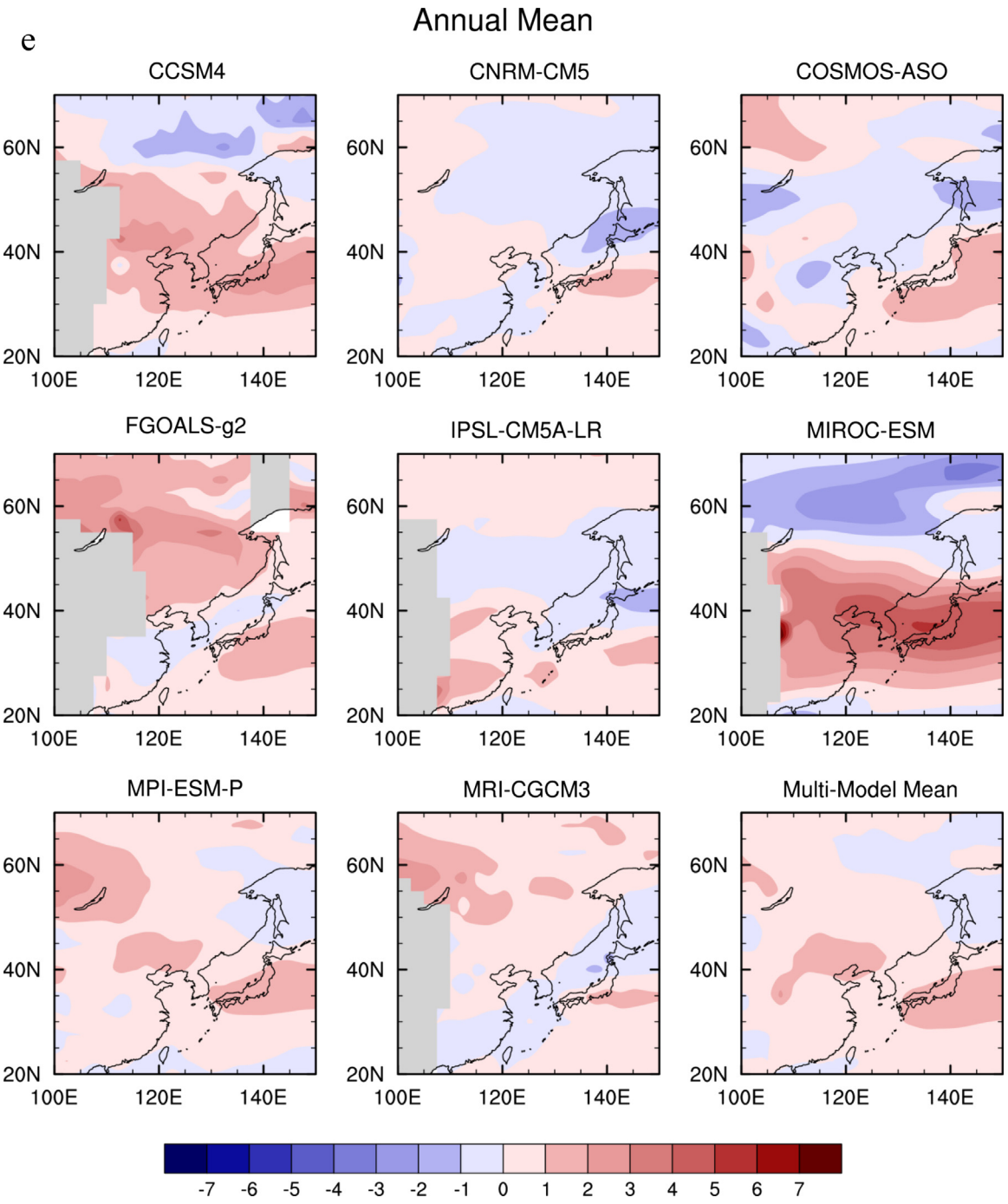

Fig. 6. (*continued*).

reconstruction are overall consistent with the climate simulation results. In particular, using principal taxa and aridity index, Yi and Kim (2010) suggested annual mean surface cooling in the LGM by about 5–6 C°. This reconstruction of surface temperature change is the same range of the simulated results in the PMIP3 models. They suggested the precipitation decreased by about 40% in the LGM, but in PMIP3 precipitation reduction was about 14%, which is much smaller than indicated by proxy evidence.

5. Summary and conclusions

This study explores the response of the climate change over Korea with LGM conditions using the coupled models of PMIP3. In the LGM, atmosphere CO_2 concentration was lower by about 80 ppm and 2–3 km of ice sheet was present over North America and northern Europe. The presence of ice sheets led to the sea level drop by about 120 m, and thus many parts of coasts were exposed land, including the Yellow Sea west of Korea. From these conditions, a cold climate is expected in the LGM, but the degree of change remains uncertain.

In order to examine the climate change over Korea in the LGM, we used 8 numerical models (CCSM, CNRM, COSMOS, FGOALS, IPSL, MIROC, MPI, and MRI). All models show substantial surface cooling over Korea, especially in winter by more than 10 C°. In summer, surface cooling is much smaller than in winter over Korea. Overall, surface LGM cooling ranges from 5 to 6 C° with a multi-model mean of −5.85 C°. This level of cooling is consistent with proxy evidence using pollen records.

Associated with the decrease in surface temperature, precipitation tends to decrease over Korea. The largest precipitation reduction occurs in winter by 56%. In spring and autumn, precipitation decreases, especially in autumn. On the other hand, precipitation increases by 12% in summer. Overall, in the LGM, precipitation decreases by about 14%.

In conclusion, in the LGM the climate was overall colder and drier than present over Korea, consistent with proxy evidence. However, there are few proxy data available over Korea, and robust comparison is limited at this stage. More reconstruction for the LGM climate using various lines of proxy evidence is required to validate the model result.

Acknowledgements

This study was supported by the projects of “Investigation of Climate Change Mechanism by Observation and Simulation of Polar Climate for the Past and Present” (PE15010) of the Korea Polar Research Institute.

References

Ballantyne, A.P., Lavine, M., Crowley, T.J., Liu, J., Baker, P.B., 2005. Meta-analysis of tropical surface temperatures during the Last Glacial Maximum. Geophysical Research Letters 32, L05712. http://dx.doi.org/10.1029/2004GL021217.

Bartlein, P.J., Harrison, S.P., Brewer, S., Connor, S., Davis, B.A.S., Gajewski, K., Guiot, J., Harrison-Prentice, T.I., Henderson, A., Peyron, O., Prentice, I.C., Scholze, M., Seppa, H., Shuman, B., Sugita, S., Thompson, R.S., Viau, A.E., Williams, J., Wu, H., 2011. Pollen-based continental climate reconstructions at 6 and 21 ka: a global synthesis. Climate Dynamics 37, 775–802.

Braconnot, P., Harrison, S.P., Kageyama, M., Bartlein, P.J., Masson-Delmotte, V., Abe-Ouchi, A., Otto-Bliesner, B., Zhao, Y., 2012. Evaluation of climate models using palaeoclimatic data. Nature Climate Change 2, 417–424.

CLIMAP, 1981. Seasonal Reconstructions of the Earth's Surface at the Last Glacial Maximum. Geological Society of America Map and Chart Series MC-36.

Cuffey, K.M., Clow, G.D., Alley, R.B., Stuiver, M., Waddington, E.D., Saltus, R.W., 1995. Large arctic temperature change at the Wisconsin-Holocene glacial transition. Science 270, 455–458.

IPCC, 2013. Climate Change 2013: the Physical Science Basis. Working Group 1 Contribution to the Fifth Assessment Report of the Intergovernmental Panel on Climate Change. Cambridge University Press, Cambridge, UK.

Jiang, D., Lang, X., 2010. Last Glacial Maximum East Asian monsoon: results from PMIP simulations. Journal of Climate 23, 5030–5038.

Jinag, D., Langm, X., Tian, Z., Guo, D., 2011. Last glacial maximum climate over China from PMIP simulations. Paleoceanography, Paleoclimatology, Paleoecology 309, 347–357.

Kim, S.-J., Flato, G., Boer, G., 2003. A coupled climate model simulation of the Last Glacial Maximum, Part 2: approach to equilibrium. Climate Dynamics 20, 635–661.

Lim, J., Nahm, W.-H., Kim, J.-K., Yang, D.-Y., 2010. Regional climate-driven C_3 and C_4 plant variation in the Cheollipo area, Korea, during the late Pleistocene. Palaeogeography, Palaeoclimatology, Palaeoecology 298, 370–377.

MARGO Project Members, 2009. Constraints on the magnitude and patterns of ocean cooling at the Last Glacial Maximum. Nature Geoscience 2, 127–132.

Shakun, J.D., Clark, P.U., He, F., Marcott, S.A., Mix, A.C., Liu, Z., Otto-Bliesner, B., Schmittner, A., Bard, E., 2012. Global warming preceded by increasing carbon dioxide concentrations during the last deglaciation. Nature 484, 49–54.

Stenni, B., Masson-Delmotte, V., Selmo, E., Oerter, H., Meyer, H., Röthlisberger, R., Jouzelb, J., Cattanib, O., Falourdb, S., Fischerg, H., Hoffmannb, G., Iacuminc, P., Johnsenh, S.J., Minsterb, B., Udisti, R., 2010. The deuterium excess records of EPICA Dome C and Dronning Maud Land ice cores (East Antarctica). Quaternary Science Reviews 29, 146–159.

Uemura, R., Masson-Delmotte, V., Jouzel, J., Landais, A., Motoyama, H., Stenni, B., 2012. Ranges of moisture-source temperatures estimated from Antarctic ice core stable isotope records over the glacial-interglacial cycles. Climate of the Past Discussions 8, 391–434.

Yi, S., Kim, J.-Y., Yang, D.-Y., Kim, J.-C., Nahm, W.-H., Yun, H.-S., 2008. Palynological implication for environmental changes in the Hanam area, Gyeonggi Province since the Last Glacial Maximum. Journal of the Geological Society of Korea 44 (5), 673–684.

Yi, S., Kim, S.-J., 2010. Vegetation changes in western central region of Korean Peninsula during the last glacial (ca. 21.1–26.1 cal kyr BP). Geosciences Journal 14, 1–10.